Atmospheric Environment 207 (2019) 1–15

Contents lists available at ScienceDirect

Atmospheric Environment

journal homepage: www.elsevier.com/locate/atmosenv

Long-term measurements of aerosol optical and physical properties over the Eastern Mediterranean: Hygroscopic nature and source regions

Ersin Tutsak, Mustafa Koçak*

Institute of Marine Sciences, Middle East Technical University, P.O. Box 28, 33731, Erdemli-Mersin, Turkey

ARTICLE INFO

Keywords:
Aerosol physical properties
Hygroscopic nature
Source regions
Eastern Mediterranean

ABSTRACT

Long-term aerosol optical and physical properties such as aerosol optical thickness and angstrom exponent were obtained from AERONET ground based sun sky radiometer located at the rural coastal Erdemli (36.6°N, 34.3°E) site in the Eastern Mediterranean from January 2000 to December 2014. Aerosol Optical Thickness (AOT) and Angstrom Exponent (α) exhibited a great short-term variability, varying up to couple of fold from day to day. The lowest AOT values was found in winter due to the removal of particles by wet deposition. Elevated AOT values with low $\alpha_{440\text{-}870}$ was observed in spring owing to sporadic mineral dust transport from North Africa and the Middle East. High AOT at 440 nm and $\alpha_{440\text{-}870}$ were characterized in summer because of high gas-to-particle conversion, sluggish air masses and absence of rain. Enhanced AOT and low α (0.7) and fine mode fraction (47%) were associated with air flow from North Africa and the Middle East with a slight decrease from 440 nm to 1020 nm, showing importance of coarse particles. Air flow from Mediterranean Sea, Eastern Europe, Western Europe and Turkey, on the other hand, showed comparatively higher α (> 1.1) and fine mode fraction (> 62%). Three classes of aerosol were identified namely non-hygroscopic dominated, moderately hygroscopic and hygroscopic dominated. Non-hygroscopic particles were dust dominated aerosol population originated from North Africa (Southern Tunisia, Western Libya, Libya/Chad border, southern Egypt northeastern Mauritania, north Mali, southern Algeria, Northwestern Niger) and the Middle East (extending from Iraq to eastern Saudi Arabia). Moderately hygroscopic particles were a mixture of mineral dust and anthropic aerosols when the dust reached receptor site after passing through industrialized and populated sites (such as Spain, France and Italy). Hygroscopic particles, however, were ascribed to nearly mesoscale formation of secondary aerosols under the prevailing summer conditions.

1. Introduction

Aerosols play a crucial role in various geophysical and geochemical processes. Atmospheric particles can alter the earth's radiation and hence climate directly by scattering and absorbing both incoming solar radiation and re-emitted radiation from the surface of the Earth to the atmosphere (Charlson et al., 1992; Haywood and Shine 1995, 1997). Aerosols can also play an essential role in hydrological cycle (Rosenfeld et al., 2008). Atmospheric particles serve as ice nuclei (IN) or cloud condensation nuclei (CNN) and they can influence the concentration and size distribution of cloud droplets; alter the distribution of rainfall and their radiative properties (Levin et al., 2005; Huang et al., 2006; Chen et al., 2007).

Direct and indirect aerosol forcing tightly depend on geographical distribution, optical properties, hygroscopic nature and types of the aerosols in relation to history of air-masses, aging process, external/internal mixing, interaction with gaseous species (heterogeneous), gas-to-particle conversion and removal either by wet or dry deposition (Patterson et al., 1977 and reference therein; Dubovik et al., 2002; Haywood et al., 2003; Eck et al., 2010; IPCC, 2013). High Aerosol Optical Thickness (AOT) values over the globe are also related to distinct processes in different regions and seasons of the year. There is a difference between Northern and Southern Hemispheres, former having higher values compared to latter mainly due to deserts (extending from the west coast of North Africa over the Middle East, central and south Asia to China, Prospero et al., 2002; Washington et al., 2003) and industrialized and populated countries (Husar et al., 1997; Kaufman et al., 2002). Relatively higher aerosol burden are found over Mediterranean particularly in MAM and JJA (up to 0.4) period because of dust transport from Sahara and Middle East desert as well as increase in secondary aerosol and biomass burning (Kubilay and Saydam, 1995; Mihalopoulos et al., 1997; Moulin et al., 1998; Kubilay et al., 2000;

* Corresponding author.
E-mail address: mkocak@ims.metu.edu.tr (M. Koçak).

https://doi.org/10.1016/j.atmosenv.2019.03.007
Received 28 September 2018; Received in revised form 8 March 2019; Accepted 11 March 2019
Available online 16 March 2019
1352-2310/

Barnaba and Gobbi, 2004; Sciare et al., 2008; Koçak et al., 2005, 2012).

A number of studies have dedicated on aerosol optical properties in the atmosphere over the Mediterranean region by applying ground-based real-time sun-photometric measurements (Kubilay et al., 2003; Meloni et al., 2006; Fotiadi et al., 2006; Pace et al., 2006; Gerasopoulos et al., 2007; Santese et al., 2008; Toledano et al., 2009). The short and long term variability in the aerosol optical thickness as well as angstrom exponent and the aerosol type have been the main foci of these articles. These studies have revealed that the change in the aerosol optical, physical properties and the aerosol type might be resulted from a combination of (a) the history of air masses back trajectories, (b) source emission strength, (c) the presence or absence of rain as well as (d) gas to particle conversion. However, to our knowledge there is a lack of scientific information about the degree of relationship between water vapor and aerosol optical thickness as a function of angstrom exponent to assess the hygroscopic state of aerosols and their possible source regions.

The current study aims to explore the optical properties of the aerosol burden in the atmospheric column over the Eastern Mediterranean. This will be achieved by using 15-year long data from the AERONET sun/sky radiometer. The unique contribution of the present study will be to (i) explore the climatology of the aerosol optical properties regarding their spectral behavior, (ii) assess the influence of meteorological parameters on the seasonal variability in aerosol optical properties, (iii) determine the effect of air flow on the aerosol optical properties and (iv) clarify the hygroscopic state of aerosols and their source regions.

2. Material and method

2.1. Study site and climatology of the region

The rural IMS-METU-Erdemli (here after Erdemli) atmospheric sampling site is located on the coastline of Eastern Mediterranean (EM), Erdemli, Turkey (36.57°N and 34.26°E, Fig. S1). **AE**rosol **RO**bit **NET**-work (AERONET) sun photometer was installed at the Institute of Marine Science, Middle Technical University Campus in December 1999 and the instrument has been operated since then. Depending on regional atmospheric dynamics, Erdemli aerosol population is mainly influenced by three aerosol sources namely; (i) anthropogenic particles from industrialized and semi-industrialized regions situated at North, (ii) mineral dust from the Sahara and Middle East Deserts located to the South and (iii) sea salt from the Mediterranean Sea (Kubilay et al., 2000; Koçak et al., 2004, 2007).

Climatically, the weather pattern of the Mediterranean region is characterized by mild, relatively wet winters and hot, dry summers (Lionello et al., 2006). Monthly average atmospheric temperature and rainfall for a 15 year period (2000–2014) at the Erdemli site are illustrated in Fig. 5h and i. The temperature presents a strong seasonal cycle with a winter minimum and a summer maximum. The average monthly temperature commences to increase from April and reaches its maximum in August (28.5 °C) and then decreases to its minimum in January (9.8 °C). On annual average, the site receives 549 mm of rain with a strong seasonal cycle. The majority of rainfall (304 mm) is observed in winter whereas very low amount of rain (11 mm) is found in summer. It is clear that the character of the sampling site is representative of the Mediterranean climate.

2.2. AERONET measurements

AERONET is a federated network of ground based sun sky radiometers operating worldwide since the middle of the 1990's. AERONET provides columnar aerosol properties such as **A**erosol **O**ptical **T**hickness (AOT), **W**ater **V**apor (WV) and inversion aerosol products. More detailed descriptions are given in Holben et al. (1998). To summarize, the sun sky radiometer makes direct Sun measurements every 15 min at 340, 380, 440, 500, 675, 870, 940 and 1020 nm. Except for 940 nm (used for retrieving WV), these measurements are then applied to calculate AOT, with an accuracy of ~0.01 for the wavelengths longer than 440 nm and ~0.02 for shorter wavelengths (Eck et al., 1999). The instrument deployed at the Erdemli site has only 440, 500 (after 2004), 675, 870 and 1020 channels for AOT measurements. AOT at 500 nm is decomposed into fine and coarse mode AOT according to the Spectral De-convolution Algorithm by O'Neill et al. (2001, 2003). The Angstrom Exponent ($\alpha_{440\text{-}870}$) is defined by the logarithms of AOT and wavelength (see Equation (1)) and it is calculated for the all wavelengths varying from 440 to 870 nm employing a lean fit between AOT and wavelength (λ) (Holben et al., 1991, 2001). The value approaching zero denotes dominance of coarse particles whereas; the value larger than 1 implies the preeminence of fine aerosol (Kaufman et al., 1994; Eck et al., 1999).

$$\alpha = -d\ ln[AOT(\lambda)]/d\ ln(\lambda) \quad (1)$$

The instrument also performs hourly sky radiance measurements in almucantar geometry at 440, 675, 870 and 1020 nm. These sky radiance measurements in conjunction with corresponding direct sun measurements are then used in inversion algorithms to derive particle size distribution (PSD) (Dubovik and King, 2000; Dubovik et al., 2006). The retrieval error in PSD is estimated to vary from 15% to 35% for the intermediate particle size range (0.1 ≤ r ≤ 0.7 μm). However, the error in PSD for small (0.05 ≤ r ≤ 0.1 μm) and large (7 ≤ r ≤ 15 μm) particle size interval may reach up to 80%.

Daily averaged aerosol optical and microphysical properties (Level 2.0, Version 2 AERONET) have been obtained for Erdemli from January 2000 to December 2014. For 15 year period, the mean observational coverage of AOT, α and WV was around 50% (n = 2712). The missing values was not only resulted from quality control but also emerged from technical malfunction of the sun photometer instrument. However, the particle size distribution was attained for 1414 days (observational coverage = 26%).

2.3. Calculation of the 5 day air mass back trajectories

Five-day back-trajectories were calculated running the HYSPLIT Dispersion Model, employing the meteorological data of the NCEP/NCAR Reanalysis Project (HybridSingle Particle Langrangian Integrated Trajectory; Draxler, 1999; Stein et al., 2015). The air masses arriving at Erdemli at 1, 2, 3 and 4 km above sea level for each day (06:00 UTC) was computed during the period between January 2000 and December 2014 (99.9% coverage). Five-day backward trajectories were selected since it extends far enough to represent the synoptic scale flow. The vertical motion of air masses was calculated using three-dimensional vertical velocity field. Based on the approach by Koçak et al. (2005, 2012), five day back trajectories arriving to Erdemli at the height of 1 km and 4 km were classified into six sectors: (i) Western Europe (WE), (ii) Eastern Europe (EE), (iii) Turkey (TUR), (iv) Middle East (MID), (v) Saharan (SAH) and (vi) Mediterranean Sea (MED) in order to evaluate the impact of airflow on aerosol optical properties (see Fig. S1). The air masses reaching at height of 2 and 3 km were omitted since the former and later were quite similar to those arriving at 1 and 4 km, respectively.

2.4. Potential source contribution function

Possible source regions of atmospheric aerosol or gases which have high concentration at a receptor site could be determined using the spatial probability distribution of pathways of air parcels that arrived at the receptor site over a time period. When the material is emitted into the air parcel from a source, it can be transported to the receptor site throughout the trajectory of the air parcel. If the endpoint of a trajectory stays at a cell of address (i,j), it is assumed that the trajectory collects the emissions from the cell. The total number of endpoints that are located in the cell is n_{ij} and there exists m $_{ij}$ points for which the measured parameter rises above a criterion value defined for this parameter, then, potential source contribution function (PSCF) is calculated using the following formula (Polissar et al., 2001).

$$PSCF_{ij} = m_{ij}/n_{ij} \tag{2}$$

In order to identify the possible source regions of non-hygroscopic, moderately hygroscopic and hygroscopic aerosols (for more details see section 3.5), PSCF was applied. The residence time probability maps (P [Bij]) were constructed when AOT values at 440 nm were larger than 0.4. Air masses back trajectories arriving at 1 km and 4 km altitudes were utilized to define source areas, by dividing the region into 2° × 2° grids (910 cells) between 20°W and 50°E and 20°N-70°N. As stated above, the air masses reaching at height of 2 and 3 km were not considered during PSCF analysis (for more information see 2.3). The small number of endpoints in a grid may generate high PSCF values with high uncertainties. After the application of binomial distribution at 95% confidence level (Vasconcelos et al., 1996), statistically significant PSCF values were retained. The PSCF values were subdivided into three classes namely: (a) weak (0.0–0.4), (b) intermediate (0.4–0.6) and (c) strong (0.6–1.0).

3. Results and discussion

3.1. General characteristics of AOT, angstrom exponent, WV and size distribution at Erdemli

Before discussing aerosol optical properties and size distribution, it is worth mentioning the probability distribution of aerosol optical thickness (AOT) measured at Erdemli from January 2000 to December 2014. Kolmogorov-Smirnov test (at 95% confidence interval) demonstrated that AOT at 440 nm distribution was lognormal (see Fig. S2). Therefore, it should be highlighted that the AOT is best represented by geometric mean value. O'Neill et al. (2000) have also shown similar distribution for AOT. Since there is a lack of such values in the literature therefore arithmetic mean values will be applied when comparing the current values obtained and those from previous studies.

Table 1 illustrates statistical summary for AOT and Angstrom Exponent (α) obtained between January 2000 and December 2014 at Erdemli site. Fig. 1 also shows corresponding mean aerosol volume size concentration throughout the study period. As can be seen from the table, arithmetic mean of AOT exhibited a remarkable decrease from 440 nm (0.30) to 1020 nm (0.12) and this reduction might be attributed to the dominance of fine particles. The arithmetic mean of AOT (440 nm) was 0.30 ± 0.18 with values ranging between 0.03 and 1.96. Geometric mean and median were identical with a value of 0.26, being 1.15 times less than that of arithmetic mean. Angstrom exponent was found to be varied between 0.03 and 2.23 with an arithmetic mean value of 1.22 ± 0.37. WV ranged from 0.19 cm to 4.54 cm with an arithmetic mean of 2.04 cm. Mean aerosol volume size concentration

Table 1
Statistical summary for aerosol optical thickness (AOT: 440, 500, 675, 870, 1020 nm), angstrom exponent ($\alpha_{440\text{-}870}$) and WV (cm) at Erdemli between January 2000 and December 2014.

Parameter	Arithmetic Mean (± δ)	Geometric Mean	Median	Minimum	Maximum
AOT_{1020}	0.12 ± 0.11	0.10	0.10	0.01	1.85
AOT_{870}	0.14 ± 0.11	0.11	0.12	0.01	1.87
AOT_{675}	0.18 ± 0.13	0.15	0.15	0.01	1.90
AOT_{500}	0.26 ± 0.16	0.22	0.22	0.01	1.94
AOT_{440}	0.30 ± 0.18	0.26	0.26	0.03	1.96
$\alpha_{440\text{-}870}$	1.22 ± 0.37	1.14	1.30	0.03	2.23
WV	2.04 ± 0.91	1.82	1.90	0.19	4.54

δ refers to standard deviation.

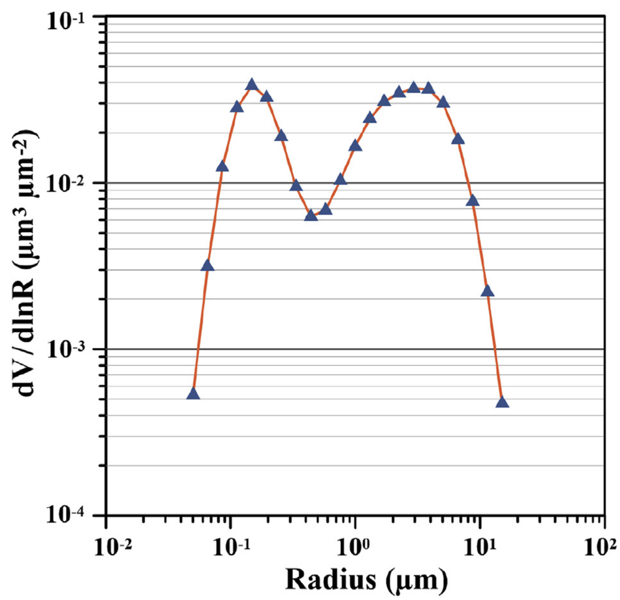

Fig. 1. Average volume size distributions from Erdemli station throughout the study period (2000–2014).

demonstrated bimodal distribution. The first peak was ascribed to fine particles (radius < 1.25 μm), majority being between 0.1 μm and 0.3 μm whilst the second peak was attributed to coarse particles, chiefly existing between 1.5 μm and 6.0 μm. Fotiadi et al. (2006) has reported two pseudo-coarse modes centered around 1.7 and 3.9 μm at Finokalai station, representing sea salt and dust particles, respectively. Unlike Finokalia, there were no pseudo-coarse modes at Erdemli rural site.

The AOT and α values from different geographical regions of the world including free troposphere, natural, rural and urban sites were used in order to assess spatial variability (see Fig. S3). Fig. 2 presents mean AOT_{440} and $\alpha_{440\text{-}870}$ for each site together with their regions and character. Mauna-Lao (Yoon et al., 2012) had the lowest AOT (0.02) since the site is above the planetary boundary layer (altitude of 3397 m). Corresponding α was 1.2, indicating contribution of stratospheric aerosols to the columnar AOT over the site. Despite Lampedusa and Forth CRETE (Mallet et al., 2013) are characterized as natural backgrounds, AOT (∼0.2) and α (∼1.1) values at these sites were comparable to those of rural sites such as Erdemli/Turkey (this study), Blida/Algeria (Mallet et al., 2013) and Kaashidoo/Maldives (Holben et al., 2001). This peculiarity might chiefly be attributed to the influence of anthropic aerosols on AOT and α when airflow originated from industrialized and semi-industrialized countries located at the northern border of the Mediterranean Sea. On the other hand, AOT and α at San Nicolas (Holben et al., 2001) were respectively 0.05 and 1.2, exhibiting the natural background character of the site. Being a natural site, AOT (0.4) and α (0.3) values at Capoverde/Sal Island were remarkably similar to those observed for Dakar (rural coastal), Banizoumbou (rural/semi-arid) and Solar Village (rural). It might be argued that AOT and α values at Sal Island, Dakar and Banizoumbou were heavily modified by mineral dust transport from Sahara desert (Holben et al., 2001; Yoon et al., 2012; Gama et al., 2015). Considering rural sites, AOT (∼0.5) and α (∼0.3) at Dakar, Banizoumbou and Solar Village were distinctly different than those of the remaining sites, demonstrating the significant effect of mineral dust particles on columnar AOT and α. The highest AOT values were observed over the urban sites in Asia, namely, Taihu (∼0.9, Xia et al., 2007) and Beijing (∼0.7, Yoon et al., 2012). It has been reported that these two Asian sites were under the heavy pressure of regional pollution (Xin et al., 2007). Except for Ilorin (urban semi-arid), the remaining urban stations had relatively high α values ranging from 1.12 to 1.68, denoting predominance of fine particles.

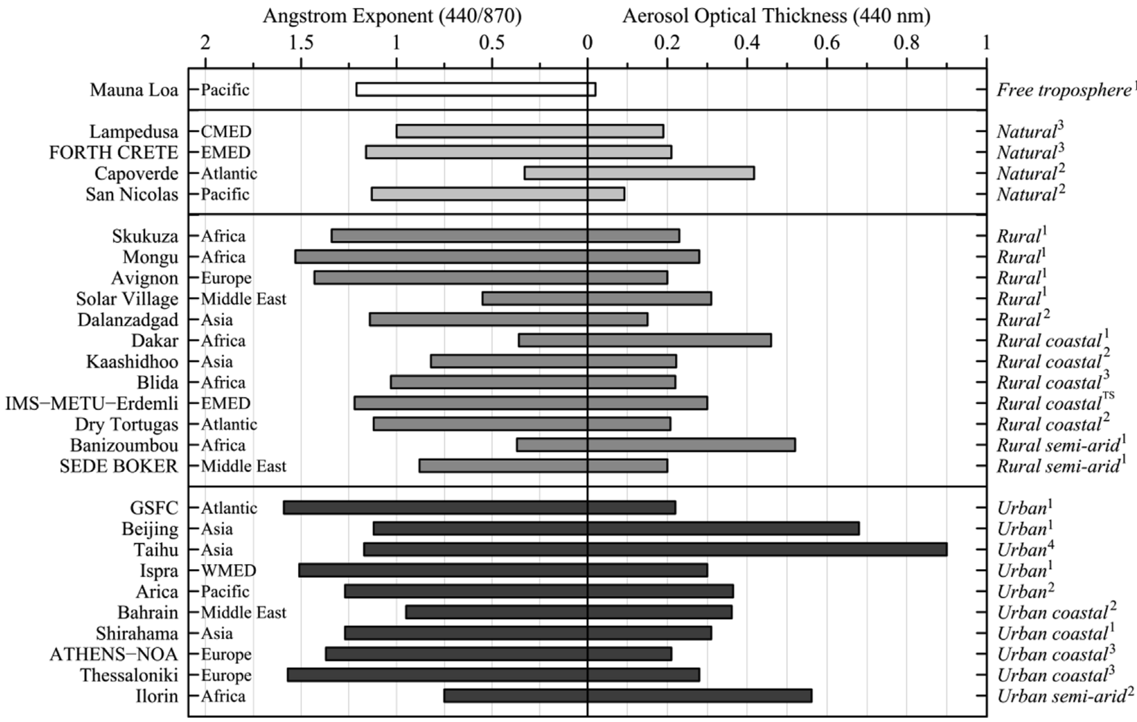

Fig. 2. Average values of AOT (440 nm) and α (440/870) at the AERONET stations ([TS] This Study; [1] Yoon et al., 2012, [2] Holben et al., 2001; [3] Mallet et al., 2013, [4] Xia et al., 2007).

3.2. Daily variability in aerosol optical thickness and angstrom exponent

Fig. 3 exhibits daily variability in aerosol optical thickness and angstrom exponent together with corresponding rainfall for Erdemli site between January 2000 and December 2014. As can be deduced from the figure, AOT and α denoted a large variability from one day to another with an order of magnitude change in their values (Holben et al., 2001; Smirnov et al., 2002; Eck et al., 2005; Giles et al., 2011).

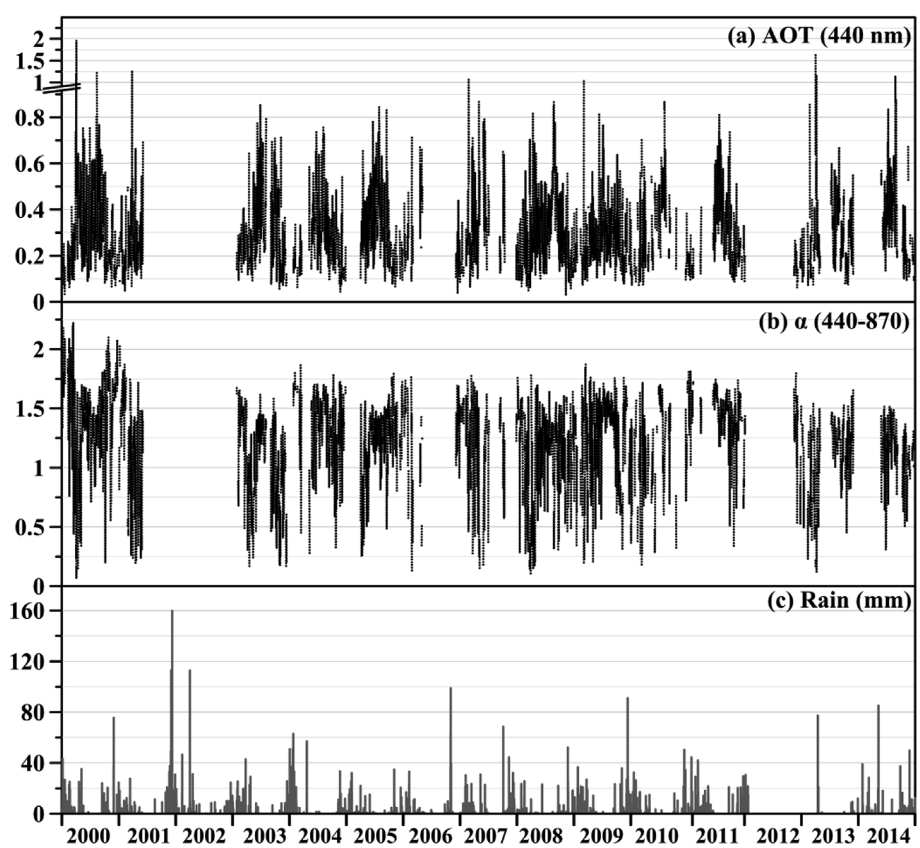

Fig. 3. Time series of daily Aerosol Optical Thickness **(a)**, Angstrom Exponent **(b)** and amount of rain **(c)** from January 2000 to December 2014.

The lowest AOT values was generally associated with rain or the day after these events since wet deposition removes aerosol particles from the atmospheric compartment efficiently (Cadle and Dasch, 1988). For instance, one of the lowest AOT was observed on 19th of January 2000 with a value 0.03. Corresponding rainfall for the same day was 15.1 mm. On 19th of January 2000 Angstrom exponent was 1.79, indicating the dominance of submicron particles.

In winter, AOT_{440} values seldom reached up to 0.6, the highest being observed on 25th of February 2007 ($AOT_{440} = 0.20 \pm 0.12$; $\alpha_{440\text{-}870} = 1.29 \pm 0.40$). Elevated AOT_{440} values were identified in spring ($AOT_{440} = 0.31 \pm 0.19$; $\alpha_{440\text{-}870} = 1.06 \pm 0.46$) and summer ($AOT_{440} = 0.40 \pm 0.17$; $\alpha_{440\text{-}870} = 1.32 \pm 0.24$) however, their corresponding $\alpha_{440\text{-}870}$ values were distinctly different. Higher AOT_{440} and lower $\alpha_{440\text{-}870}$ were particularly detected during spring months (March, April and May) when the air masses back trajectories originated from deserts situated at North Africa and the Middle East. Studies have clearly shown that aerosol population in the Eastern Mediterranean is considerably affected by sporadic mineral dust pulses mainly occurring in transitional seasons (Kubilay and Saydam, 1995; Kubilay et al., 2000, 2003). Enhanced AOT_{440} and $\alpha_{440\text{-}870}$ were identified throughout summer owing to prevailing weather conditions. Higher gas to particle conversion, sluggish airflow and the lack of rain allow accumulation of aerosol particles in the atmosphere over the Eastern Mediterranean (Koçak et al., 2007; Dayan et al., 2017 and references therein). Consequently, higher values of AOT might be categorized into three main classes: (a) dust dominated, (b) mixed (dust/pollution) and (c) pollution dominated. During the study period, 46 cases were identified as dust dominated episodes ($AOT_{440} > 0.5$; $\alpha_{440\text{-}870} < 0.5$) with mean AOT_{440} and $\alpha_{440\text{-}870}$ values of 0.74 ± 0.30 and 0.25 ± 0.12, respectively. From 2000 to 2014, 65 and 253 cases were respectively characterized as mixed ($AOT_{440} = 0.64 \pm 0.12$, $\alpha_{440\text{-}870} = 0.74 \pm 0.15$; $AOT_{440} > 0.5$; $\alpha_{440\text{-}870} = 0.5$–$1.0$) and pollution dominated events ($AOT_{440} = 0.62 \pm 0.11$, $\alpha_{440\text{-}870} = 1.40 \pm 0.17$; $AOT_{440} > 0.5$; $\alpha_{440\text{-}870} > 1.0$). These events exhibited that such episodes were mainly associated with pollution dominated aerosol type (~70%). Corresponding examples for each event are presented in Fig. 4a, b and c (see Fig. S4).

3.2.1. Dust dominated

One of the highest AOT was observed on 2nd of April 2013 with a value of 1.67 (Fig. 4a). On March 30, AOT (440 nm) and α were respectively found to be 0.22 and 1.08. From March 30 to April 1, AOT (440 nm) tripled over the Erdemli in contrast, α value decreased five times. The initial signal of this dust event was clearly detected by the sun photometer on April 1. During the next day, AOT (α) incremented (reduced) 2.6 (1.5) times compared to former day, demonstrating intensification of the dust episode over the site. Ozone Mapping Instrument Aerosol Index (OMI-AI) satellite image for April 1 (Fig. S5a) demonstrated dense dust cloud over the Levantine basin however; the thickness of dust was less over the Northeastern Levantine, OMI-AI being around 1. During this day, OMI-AI values reached up to 4 between coordinates 30°N – 37°N and 27°E – 30°E. Within a day (Fig. S5b), the dust cloud became less apparent over the South Levantine Basin whilst the intensity of the dust cloud enhanced in the atmosphere over the Northeastern Levantine, especially at Turkish coastline. For instance, AI on April 2 over Erdemli site doubled compared to that of observed on April 1. Five-day back trajectories also supported mineral dust transport from deserts located at the Middle East and North Africa. On April 1 (Fig. S5a), trajectories at 1, 2 and 3 km denoted that Erdemli site was under the influence of airflow from the Middle East whereas; trajectory at 4 km showed air mass transport from North Africa. Next day, lower layer trajectories (1 and 2 km, Fig. S5b) demonstrated that site was still affected by airflow from south east. Therefore, prevailing air mass transport mainly from the Middle East and lesser extent from North Africa as well as the absence of rain resulted in enhanced AOT over the Erdemli site. Another example for dust dominated event was observed on 7th of March 2009 when AOT_{440} and α were respectively 1.1 and 0.19 (see Fig. S6). Air masses back trajectories exhibited air flow from the Middle East at altitudes of 1 km whilst the air masses reaching at 2, 3 and 4 km heights originated from the North Africa, suggesting the site was under the influence of deserts located in the Middle East and the North Africa at the same time. OMI-AI satellite image for March 7 also supported the presence of the dust plume over the Eastern Mediterranean, with AI values exceeding 2.5 particularly over the Erdemli.

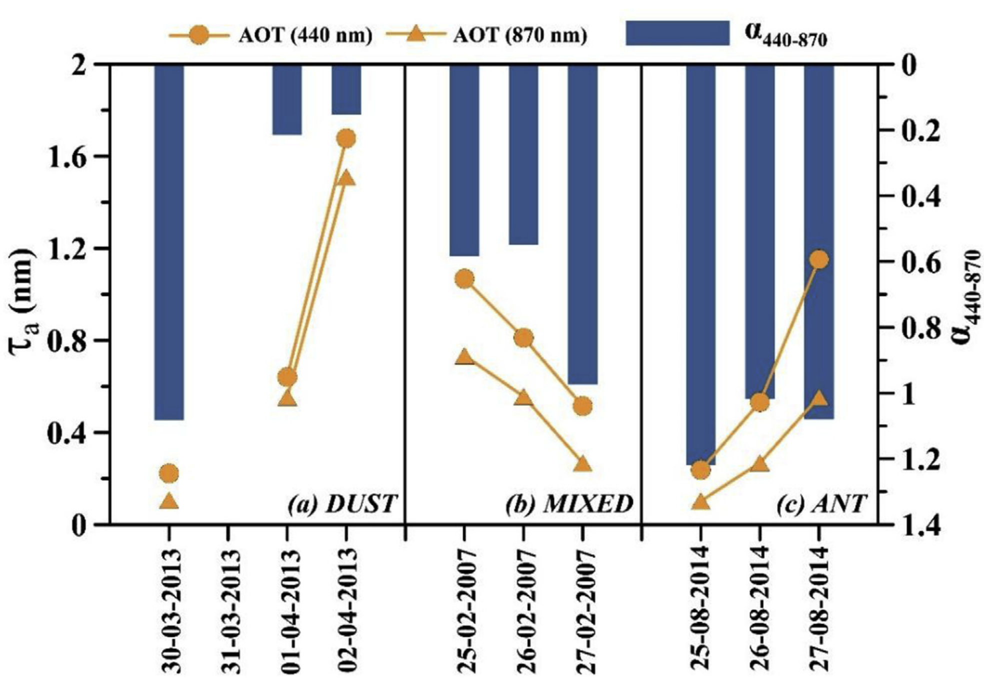

Fig. 4. Variability in Aerosol Optical Thickness and Angstrom Exponent (α) during dust **(a)**, mixed **(b)** and pollution events **(c)** at Erdemli.

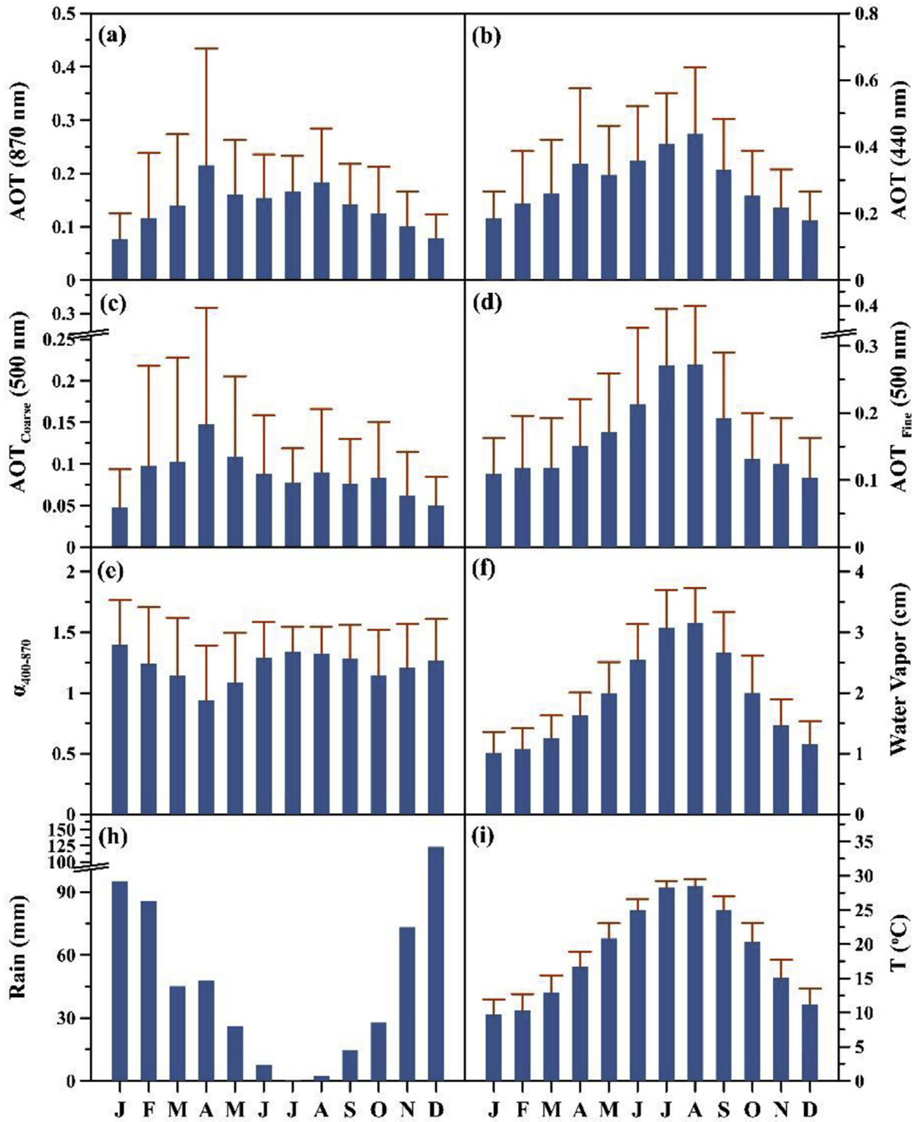

Fig. 5. Mean monthly values of AOT_{440} **(a)**, AOT_{870} **(b)**, coarse mode AOT **(c)** and fine mode AOT **(d)** at 500 nm, $\alpha_{440\text{-}870}$ **(e)**, water vapor **(f)**, total rain **(h)** and temperature **(i)**. The bars represent standard deviations.

3.2.2. *Mixed event*

Mixed dust event was characterized from February 25 to 27, 2007 (Fig. 4b). On 25 February, the influence of the mineral dust first detected by sun photometer with an AOT_{440} (α) value of 1.06 (0.58). The following day AOT_{440} was found to decrease to 0.81, together with a slight reduction in α value. On 27 February, AOT_{440} continued to decreased, attaining value of 0.52 with a twofold decrement compared to the initial AOT_{440} value of the case nonetheless, α value increased 1.9 times from previous two days, reaching value of 0.97. OMI-AI satellite image for 25 February indicated a large dust plume over Eastern Mediterranean extending from 32°N – 38°N to 25°E – 35°E, which AI values ranging from 2.0 to 3.0 were observed over the region (Fig. S7). During the next day, dust plume became less intense and on 27 February dust cloud disappeared over the region. Considering the back trajectories (Fig. S7), air masses originated from North Africa (passing over Egypt) arrived to the site at 2, 3 and 4 km altitudes on 25th February, whilst the back trajectory for 1 km altitude indicated airflow over Turkey. During the next day, air flow for 1 km altitude showed a transport from region located over Ukraine, middle Black Sea and Turkey whereas air masses at upper levels (3 and 4 km) advected to the site from North Africa. Back trajectories for 27 February indicated air flow at upper levels from North Africa terminated and started to come from northwest. The second example were identified on 14th of May 2010 with AOT_{440} and α values of 0.54 and 0.71, respectively (see Fig. S8). Air masses arriving at 1 and 2 km resulted from Western Sahara and reached the site after sweeping Italy, the Balkans and highly populated as well as industrialized the region of Marmara, including the Mega City Istanbul. On the other hand, the air masses at 3 and 4 km altitude denoted air flow from Western Sahara without interacting urban and/or industrialized areas. OMI-AI diagram also showed dust activity in the North Eastern Mediterranean Basin, ranging from 1.5 to 2.5.

3.2.3. *Pollution dominated event*

The third event was described from August 25 to 27, 2014 (Fig. 4c). On 25 August, AOT_{440} and α were respectively found to be 0.24 and 1.21 by sun photometer. Next day, AOT_{440} almost doubled over the Erdemli whereas α was found to decrease by 10%, reaching the value of 1.07. On 27 August, AOT reached the highest value of the event, attaining value of 1.15 with a fivefold increment from 25 to 27 August. Nonetheless, α was found to be 1.08 and the change in Angstrom Exponent from 25 to 27 August was only about 10%, all values being higher than 1. MODIS-Terra (Moderate Resolution Imaging Spectrometer) AOD satellite image for 25 August indicated low thickness over site (see Fig. S9). Then, next day it started to increase and on 27 August, attained the value of 0.8 with a four-fold increase from 25 to 27 August. Corresponding five-day back trajectories exhibited that air masses arrived to the site at all altitudes from north and northwest on 25 August (see Fig. S9). Next day, lower layers (1 and 2 km) back trajectories was related to air flows coming from northern sector whereas, upper layers (3 and 4 km) back trajectories were associated with air mass transport from south. On 27 August, trajectory at 1 km indicated the site still remained under influence of air mass transport from the region located over eastern Black Sea and Turkey. On the other hand, trajectory at 2, 3 and 4 km pointed the air mass transport from southwest. It should be noted that on 26 and 27 August, air masses reached the site at 3 and 4 km, descending vertically from further height levels nonetheless, the trajectory at 1 km on 26 August and trajectories at 1 and 2 km on 27 August indicated that air masses arrived to the site at corresponding heights, ascending vertically from ground levels (see Fig. S10). The case observed on 14th of July 2013 can be given as another example for pollution dominated episodes with corresponding AOT_{440} and α values of 0.60 and 1.43 (see Fig. S11). Air masses back trajectories exhibited that all air flows were arising from industrialized, semi-industrialized and populated areas located on the North of the Mediterranean Sea. OMI-AI satellite image illustrated that the Eastern Mediterranean was not under the influence of dust particle, being less than 0.5.

3.3. Seasonal variability in aerosol optical thickness and angstrom exponent

Monthly arithmetic mean and standard deviations for aerosol optical thickness (440 and 870 nm, coarse and fine at 500 nm), angstrom exponent, water vapor together with local rain amount and temperature are presented in Fig. 5. The lowest values of AOT (440, 870 nm, fine and coarse) were found in winter. The minimum in winter might be ascribed to four main processes namely (a) efficient removal of aerosol burden from the atmospheric compartment by rain, (b) reduced gas to particle conversion due to cloud cover and incoming solar flux, and (c) less frequent dust transport from the Middle East and North Africa (d) emission strength of sources (Kubilay et al., 2003; Fotiadi et al., 2006; Gerasopoulos et al., 2007). Notwithstanding, there was a distinct difference in the seasonal cycle of $AOT_{440,}$ $AOT_{870,}$ AOT_{coarse} and AOT_{fine}. To begin with AOT_{870} (AOT_{coarse}), monthly arithmetic mean gradually increased from January to March and reached its maximum in April with a value of 0.22 (0.17). Arithmetic mean of AOT_{870} (AOT_{coarse}) then reduced 40% (60%) from April to June. AOT_{870} (AOT_{coarse}) demonstrated 20% (only 5%) enhancement from June to August. Mean AOT_{870} (AOT_{coarse}) abruptly declined from 0.18 (0.09) to 0.08 (0.05) between August and December. On the whole, arithmetic mean of AOT_{440} (AOT_{fine}) illustrated piecemeal augmentation from January to August, attaining its maximum with a value of 0.44 (0.27). After that, mean AOT_{440} (AOT_{fine}) began to decrease and achieved its winter values in December (AOT_{440} ~ 0.18, AOT_{fine} ~ 0.10). Monthly mean of $\alpha_{440\text{-}870}$ denoted steady decrease from 1.40 to 0.94 between January and April. Then $\alpha_{440\text{-}870}$, raised about 40%, reaching value of 1.30 in June whilst $\alpha_{440\text{-}870}$ did not pointed out remarkable change from June to December. The seasonal cycle of water vapor, on the other hand, was similar to that of observed for AOT_{fine}. Monthly mean water vapor exhibited substantial increase from January (1.0 cm) to August (3.2 cm) and later its monthly values drastically dropped to 1.1 cm towards end of the year.

The AOT versus $\alpha_{440\text{-}870}$ gives qualitative information about the aerosol burden and particle size and hence it is a useful tool to distinguish antropic from natural aerosols (Eck et al., 2001; Holben et al., 2001; Smirnov et al., 2002; Fotiadi et al., 2006). Seasonal scatter diagrams for AOT_{440} versus $\alpha_{440\text{-}870}$ together with the frequency of occurrence of these two parameters are depicted in Fig. 6. As can be deduced from scatter plots, winter (DJF) and spring (MAM) showed a strong trend of increase in AOT_{440} values as $\alpha_{440\text{-}870}$ decreases, though, summer (JJA) and fall (SON) exhibited a very weak trend of reduction in AOT_{440} values with decreasing $\alpha_{440\text{-}870}$. Seasonal histograms for AOT_{440} and α_{440}.870 also denoted distinct difference. The frequency of occurrence histogram of AOT_{440} showed gradual shift toward higher values from winter to summer and it decreased from summer to fall. In winter, spring and fall, the AOT_{440} probability distributions exhibited peak values of 0.1–0.2 (51%) 0.2–0.3 (35%) and 0.1–0.2 (32%), respectively, whereas AOT_{440} illustrated peak value of 0.3–0.4 (25%) in summer. The AOT_{440} frequency distributions clearly showed that the atmosphere over the Eastern Mediterranean was more turbid in summer than those observed for the remaining seasons. As stated before, this might be result of higher gas to particle conversion, sluggish airflow and lack of rain. The frequency of occurrences histogram for $\alpha_{440\text{-}870}$ displayed relatively narrow peak from 1.1 to 1.6 in summer (77%) and fall (56%) on the other hand, only few percent had values less than 0.5 (summer: 1.2%, fall: 3.5%), showing that fine particles were dominant. Unlike summer and fall, the $\alpha_{440\text{-}870}$ probability distribution was rather broader (wide range particle size) in spring, 16% being lower than 0.5. About 50% of $\alpha_{440\text{-}870}$ < 0.5 values had AOT_{440} larger than 0.4, implying the transport of mineral dust from North Africa and Middle East deserts (Koçak et al., 2004). The remaining episodes might be attributed to weak dust events and/or sea salt. Furthermore, more than 16% of the $\alpha_{440\text{-}870}$ in winter, spring and fall ranged from 0.5 to 1.0, suggesting mixed mineral dust and anthropic particles. Therefore, it might be argued that the aerosol population was comparatively more diverse in spring compared to winter, summer and fall.

Correlations between variables illustrate the degree to which they together. In order to clarify monthly relationship between AOT, $\alpha_{440\text{-}870}$, water vapor and local meteorological parameters, namely temperature and rain were used. The individual monthly means from 2000 to 2014 were applied to carry out correlation analysis when the number of data were at least 15 days per month, remaining 98 out of 132 months. The significance level of the correlation coefficient is considerably influenced by the number of the sample. Therefore, even a small correlation coefficient can be considered as statistically significant in populations with a high number of samples. Subsequently, Three different terms will be utilized during the interpretation of correlation coefficients: (a) weak correlation (r = 0–0.3), (b) moderate correlation (r = 0.3–0.6) and (c) strong correlation (r = 0.6–1.0).

The correlation coefficients between aforementioned variables are given in Table 2. The obtained correlation coefficients indicated that water vapor, temperature and total rain amount significantly modified the seasonality of aerosol physics in the atmosphere over the Erdemli. Rain was moderately correlated with water vapor (r = −0.37), denoting the removal of the water from the atmosphere column in the form of precipitation. Except for AOT_{coarse}, there were negative correlation between rain amount and AOT_{870}, AOT_{440} and AOT_{fine}. However, the correlation coefficients were only moderate for AOT_{440} (r = −0.30) and AOT_{fine} (r = −0.42). In addition, AOT_{440} (r = 0.63) and AOT_{fine} (r = 0.70) showed strong correlation coefficients with temperature. Therefore, during winter month's AOT_{440} and AOT_{fine} decreased not only due to the removal of particles from atmospheric compartment but also because of less efficient gas to particle conversion (e.g. cloudy days, inferior incoming solar influx). Influence of rain on AOT_{870} (r = −0.12) and AOT_{coarse} (r = 0.11) was not important and hence this might be ascribed to the mechanical formation of coarse particles and their source strength. For example, atmospheric sea salt production especially increases in rainy winter months owing to more active and frequent storms (Marks, 1990; O'Dowd, C. D. and M. H. Smith, 1993). Furthermore, in spite of considerable rain, the mineral dust transport from desert sources to the receptor site has primarily been determined in spring (March, April and May) when the prevailing conditions are more favorable for the Saharan cyclones (Kubilay et al., 2000). Angstrom Exponent indicated strong negative correlation with AOT_{coarse} (−0.77) although it showed moderate negative correlation coefficient with AOT_{870} (−0.49). Considering these relationship, it might be note that the seasonality of $\alpha_{440\text{-}870}$ was mainly controlled by the existence

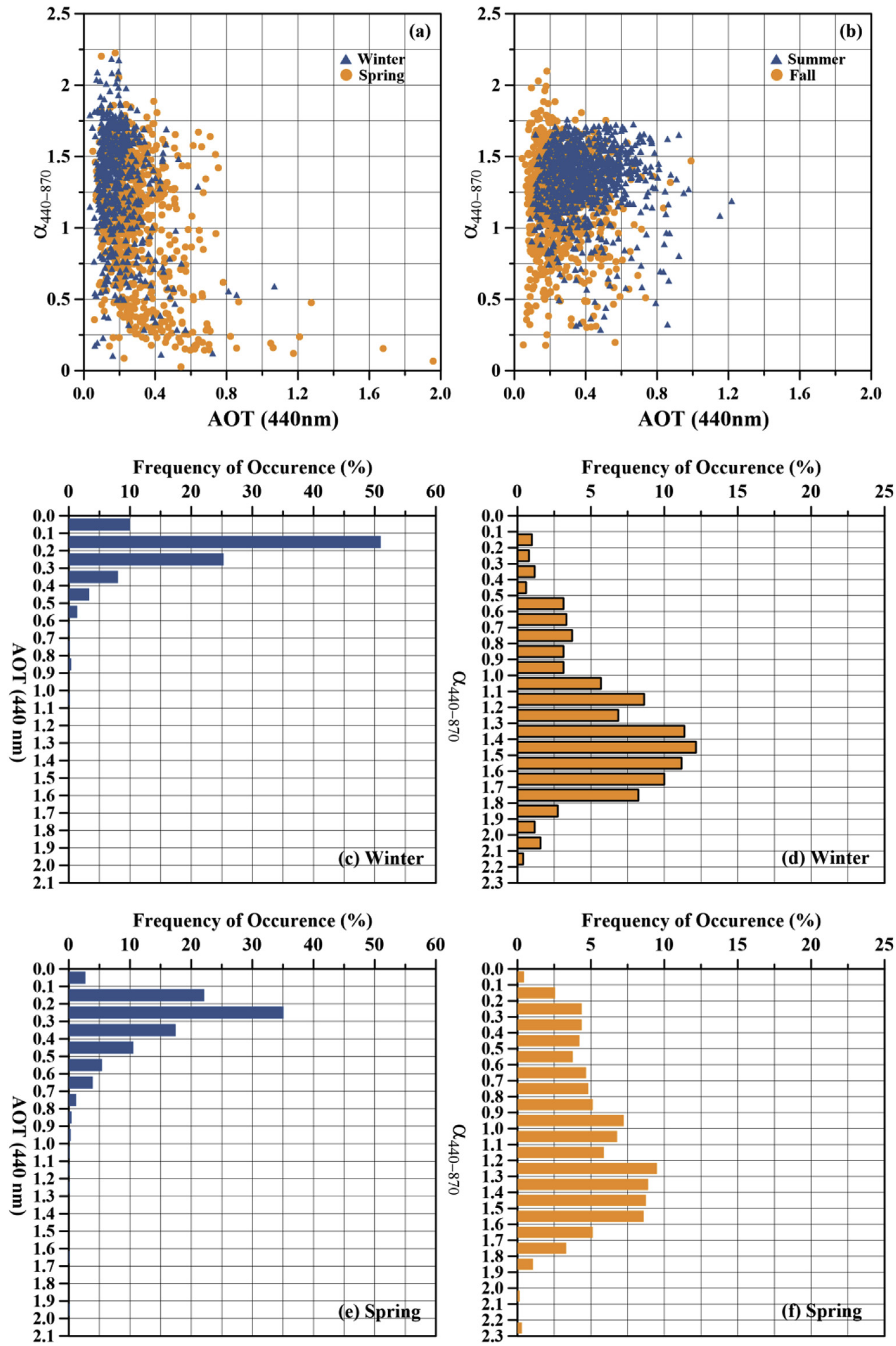

Fig. 6. Seasonal scatter plot of AOT_{440} versus $\alpha_{440\text{-}870}$ **(a–b)** and frequency of occurrence of AOT_{440} and $\alpha_{440\text{-}870}$ for winter **(c–d)**, spring **(e–f)**, summer **(g–h)**, and fall **(i–j)**.

of coarse particles.

3.4. Influence of air flow on aerosol optical properties

The origin of air masses influence the aerosol optical thickness and angstrom exponent (Smirnov et al., 1995, 1996; Eck et al., 2008; Giles et al., 2011). To assess the influence of air flow on aerosol optical properties, the categorization of trajectories were utilized. The Kruskal-Wallis (K-W) test was applied to test for the presence of significant differences in aerosol optical properties namely aerosol optical thickness at 440, 675, 870 as well as 1020 nm, angstrom exponent and fine fraction (%) classified according to air masses. Table 3 and Fig. 7 illustrate statistical summary of the AOT, $\alpha_{440\text{-}870}$ and FF (%) for each air flow sector.

3.4.1. Air flow reaching at altitude of 1 km

Table 3.a and Fig. 7 illustrate statistical summary of the AOT, $\alpha_{440\text{-}870}$ and FF (%) for each air flow sector at 1 km. Application of Kruskal-

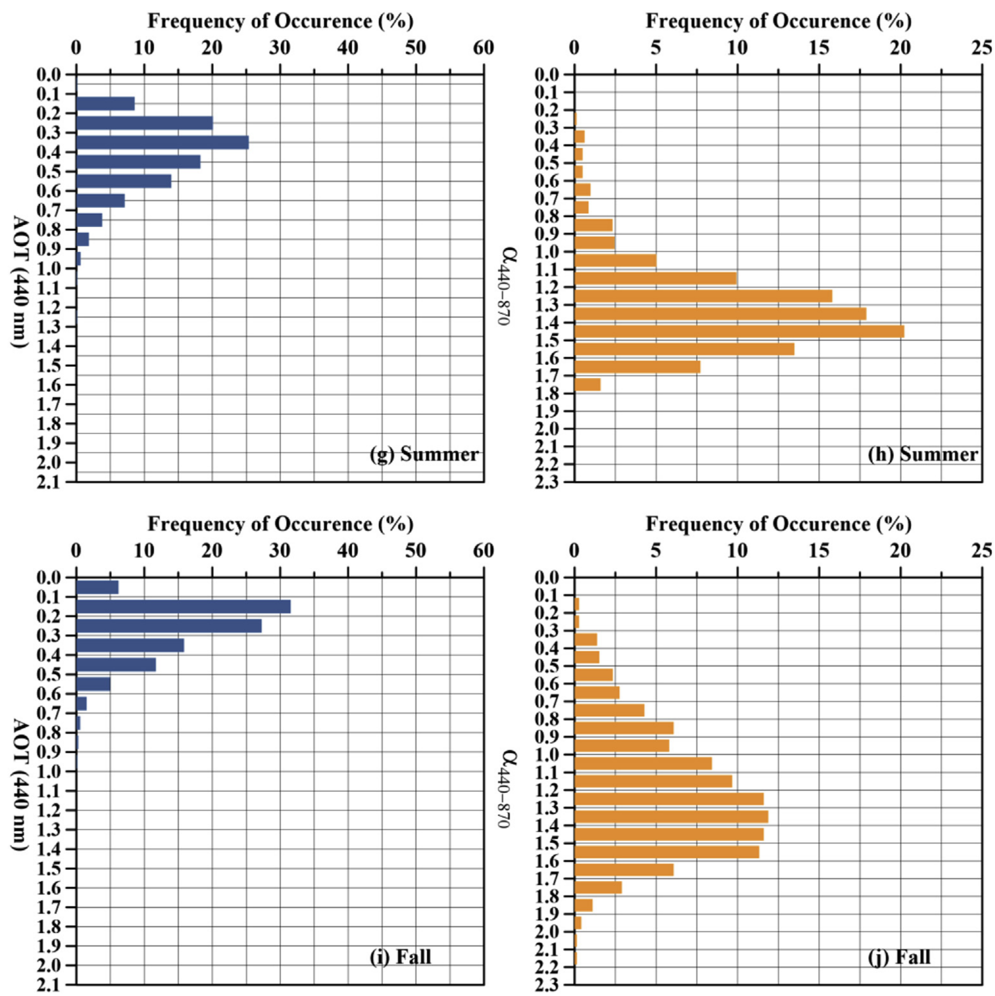

Fig. 6. (*continued*)

Wallis test exhibited that aerosol optical thicknesses at 440 nm for MID, SAH and TR were not statistically different. Likewise, AOT for MED, EE and WE was found to be comparable and they were statistically not different. AOT for MID, SAH and TR was at least 15% larger than those observed for MED, EE and WE. On the other hand, mean AOT for air flow showed dramatic difference with increasing wavelength. For MID and SAH air flow, AOT exhibited slight decrease from 440 nm to 1020 nm, indicating dominance of coarse particle. Angstrom exponent and the percent contribution of fine fraction in these air masses were also support the above statement, former and later being around 0.75 and 47%, respectively. Conversely, AOT for MED, EE, WE and TR denoted almost 65% decrease between 440 nm and 1020 nm since aerosols arising from these air flow sectors were mainly associated with fine mode ($\alpha_{440\text{-}870} > 1.1$ and FF > 62%, see Table 3.a and Fig. 7). Results from K-W test demonstrated statistically significant difference for AOT between MID, SAH and MED, EE, WE as well as TR at 675 nm, 870 nm and 1020 nm, first two sectors being approximately 2 times higher than the remaining air flows. Furthermore, angstrom exponent and the percent contribution of fine fraction were remarkably lower for MID and SAH compared to air flow originated from MED, EE, WE and TR.

3.4.2. Air flow reaching at altitude of 4 km

The results from K-W test for 4 km air flow was less dramatic relative to 1 km, suggesting influence of different air masses in the atmospheric column at the same time. For example, the air flow reaching at 4 km altitude from SAH sector exhibited diverse air masses transport at 1 km. Correspondingly, 18, 5, 17, 21, 27 and 12% of trajectories at 1 km altitude were associated with air flow from EE, MED, MID, SAH,

Table 2

Matrix correlation for individual monthly (n = 98) AOT (440 nm), AOT (870 nm), fine as well as coarse AOT, α (440/870), water vapor (WV), temperature (T) and total rain (R). Bold and italic characters illustrate strong and moderate correlation coefficients, respectively.

	AOT_{870}	AOT_{440}	AOT_{coarse}	AOT_{fine}	$\alpha_{440\text{-}870}$	WV	T	R
AOT_{870}	1.00							
AOT_{440}	**0.80**	1.00						
AOT_{coarse}	**0.85**	*0.38*	1.00					
AOT_{fine}	*0.49*	**0.91**	−0.03	1.00				
$\alpha_{440\text{-}870}$	*−0.49*	0.02	**−0.77**	*0.52*	1.00			
WV	*0.38*	**0.76**	0.01	**0.87**	0.27	1.00		
T	*0.31*	**0.63**	0.02	**0.70**	0.22	**0.90**	1.00	
R	−0.12	*−0.30*	0.11	−0.42	−0.11	*−0.37*	*−0.41*	1.00

Table 3
Arithmetic means and standard deviations for AOT, AE and fine mode fraction as a function of air flow for 1 km **(a)** and 4 km **(b).**

a)	WE (n = 327) Mean ± Std	EE (n = 1028) Mean ± Std	TR (n = 771) Mean ± Std	MID (n = 147) Mean ± Std	SAH (n = 194) Mean ± Std	MED (n = 244) Mean ± Std
AOT_{440}	0.27 ± 0.15	0.28 ± 0.16	0.34 ± 0.18	0.36 ± 0.25	0.35 ± 0.20	0.29 ± 0.15
AOT_{675}	0.17 ± 0.11	0.15 ± 0.09	0.20 ± 0.11	0.28 ± 0.24	0.26 ± 0.19	0.17 ± 0.09
AOT_{870}	0.13 ± 0.09	0.11 ± 0.07	0.15 ± 0.09	0.25 ± 0.24	0.23 ± 0.18	0.13 ± 0.07
AOT_{1020}	0.12 ± 0.09	0.09 ± 0.06	0.12 ± 0.08	0.23 ± 0.24	0.21 ± 0.17	0.11 ± 0.06
$\alpha_{440\text{-}870}$	1.1 ± 0.4	1.3 ± 0.3	1.3 ± 0.3	0.8 ± 0.4	0.8 ± 0.4	1.3 ± 0.3
FF	0.62 ± 0.17	0.73 ± 0.11	0.71 ± 0.14	0.49 ± 0.19	0.47 ± 0.19	0.68 ± 0.13

b)	WE (n = 1508) Mean ± Std	EE (n = 325) Mean ± Std	TR (n = 273) Mean ± Std	MID (n = 81) Mean ± Std	SAH (n = 511) Mean ± Std
AOT_{440}	0.30 ± 0.16	0.21 ± 0.11	0.33 ± 0.17	0.46 ± 0.26	0.37 ± 0.20
AOT_{675}	0.17 ± 0.11	0.11 ± 0.06	0.18 ± 0.10	0.30 ± 0.18	0.26 ± 0.17
AOT_{870}	0.13 ± 0.09	0.08 ± 0.04	0.13 ± 0.08	0.24 ± 0.15	0.22 ± 0.16
AOT_{1020}	0.11 ± 0.08	0.07 ± 0.03	0.11 ± 0.07	0.21 ± 0.14	0.20 ± 0.15
$\alpha_{440\text{-}870}$	1.3 ± 0.3	1.4 ± 0.3	1.4 ± 0.3	1.1 ± 0.4	0.9 ± 0.4
FF	0.70 ± 0.14	0.73 ± 0.12	0.74 ± 0.12	0.62 ± 0.17	0.55 ± 0.20

FF, std denotes fine mode fraction at 500 nm and standard deviation, respectively.

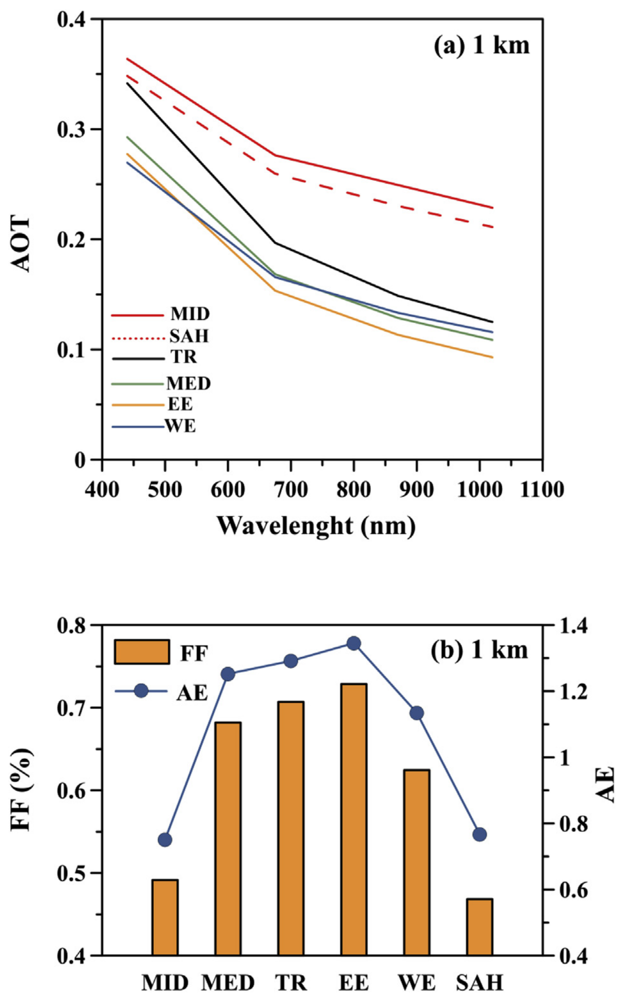

Fig. 7. Variability in aerosol optical thickness **(a)**, fine fraction and angstrom exponent **(b)** according to the clusters at 1 km.

TR and WE when air masses arriving at 4 km altitude from SAH. Fig. 8a and b show AOT at 1020 nm and angstrom exponent according to air masses transport from EE, MED, MID, SAH, TR and WE for SAH air flow at 4 km altitude. As expected, K-W test exhibited dramatic difference for air masses categories. For AOT at 1020 nm, air masses back trajectories arising from SAH and MID was remarkably larger (at least 30%) than

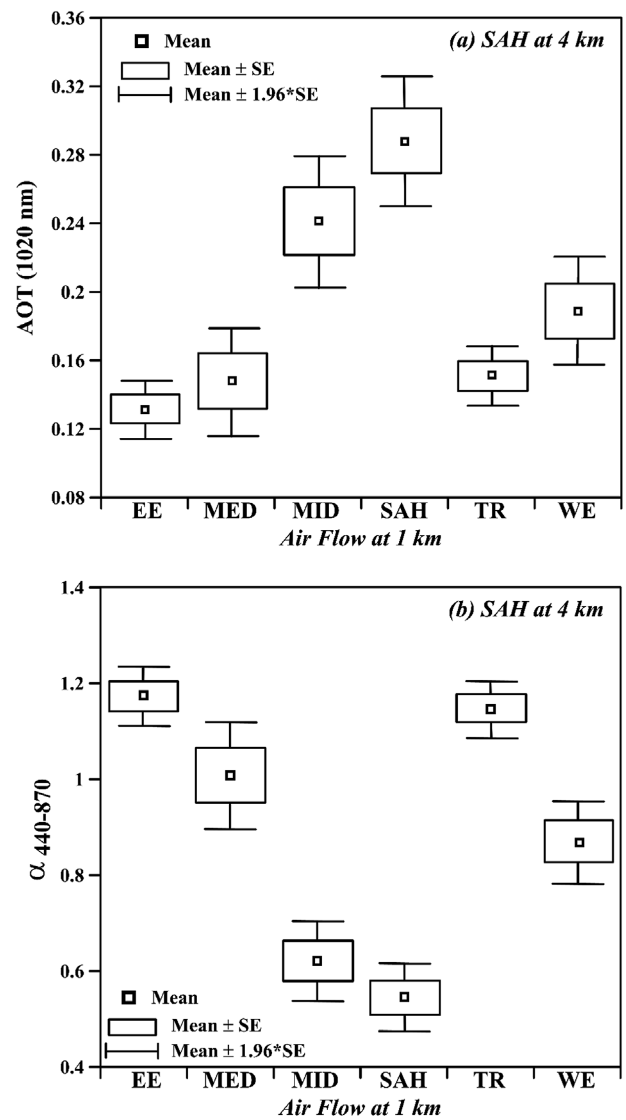

Fig. 8. Bow-whisker plot of AOT at 1020 nm **(a)** and angstrom exponent **(b)** according to air masses transport from EE, MED, MID, SAH, TR and WE at 1 km when air masses arriving at 4 km altitude from SAH.SE refers to standard error.

those observed for the remaining air flow sectors. Angstrom exponent of MID and SAH was also statistically different than the other sectors, the former group being less than 0.62 and the latter group being higher than 0.86. Therefore, it might be suggested that the impact of mineral dust transport was less obvious in the atmospheric column when the air flows originated from industrialized and populated areas due to the dilution effect of anthropic aerosols.

3.5. Hygroscopic nature of aerosols and their potential source

In order to investigate relationship between water vapor and AOT, value of $\alpha_{440\text{-}870}$ has generally been classified into groups namely $\alpha_{440\text{-}870} > 0.70$ (or 0.75) and $\alpha_{440\text{-}870} < 0.70$ (or 0.75) since the threshold for $\alpha_{440\text{-}870}$ tentatively differentiate anthropogenic dominated aerosol population from natural (Smirnov et al., 2002; Eck et al., 2008). It should be noted that the application of such an arbitrary threshold might not fully separate aerosol type from the one another, yet this type of application is inevitable because it provides simplicity to explore hygroscopic growth or hygroscopic nature of aerosol type. Nevertheless, in this study the relationships between these two variables were investigated for three different α classes specifically: (i) $\alpha_{440\text{-}870} < 0.5$, (ii) $0.5 < \alpha_{440\text{-}870} < 1.0$ and (iii) $1.0 < \alpha_{440\text{-}870} < 2.0$. The first group was dominated by coarse particles, accounting of 75% of AOT_{440} whilst the second group was equally influenced by coarse (~51%) and fine (~49%) particles. In contrast, the third class was dominated by fine particles, elucidating 80% of the observed AOT_{440}. The relationship between AOT_{440} and water vapor is shown in Fig. 9. The logarithmic fit was found to explain much more of the variance between AOT_{440} and water vapor compared to linear fit. In general, AOT_{440} increased with increasing water vapor, however; the degree of relationship between AOT_{440} and water vapor for each group was different. The correlation coefficient between two variables was found to increase with enhancing α. The relationship for the first group was weak ($R^2 = 0.13$, $p < 0.0002$, Fig. 9a), suggesting that the particles in this group exhibited the least hydroscopic growth compared to the remaining groups. The relationship for the second group was moderate ($R^2 = 0.36$, $p < 0.0002$, Fig. 9b), denoting moderate hydroscopic growth. As it is well known, the sea salt has a high hygroscopicity (Petters and Kreidenweis, 2007) with a small $\alpha_{440\text{-}870}$. Thus, the first group might be influenced by sea spray. The sea salt is produced by bubble bursting which commences at a wind speed of about 3–4 m s^{-1} (O'Dowd et al., 1997) and therefore its production is greatly related to the local wind speed. In order to assess the impact of sea salt on these groups the relationship of wind speed with water vapor and AOT was investigated when the local wind originated from sea. The regression analysis did not reveal any statistically significant relationship between wind speed and AOT (first group: $r = -0.1$; for second group: $r = -0.3$) as well as water vapor (first group: $r = -0.1$; for second group: $r = -0.02$). It is seem that the aerosols in the first group was mainly dominated by mineral dust with a low hygroscopicity (Koehler et al., 2009). Moderate hygroscopic property of the second group might be ascribed to mixing of different type aerosols such as mineral dust and anthropogenic sulfates, nitrates and/or organic acids (Koçak et al., 2007, 2012). If the first and second group were originated from distinct aerosol populations, then the former would show less interaction with anthropogenic sulfates, nitrates and/or organic acids relative to later. The ratio of $nssSO_4^{2-}/nssCa^{2+}$ is a useful tool to investigate such an interaction. The ratio of 0.4 ± 0.1 for $nssSO_4^{2-}/nssCa^{2+}$ has been

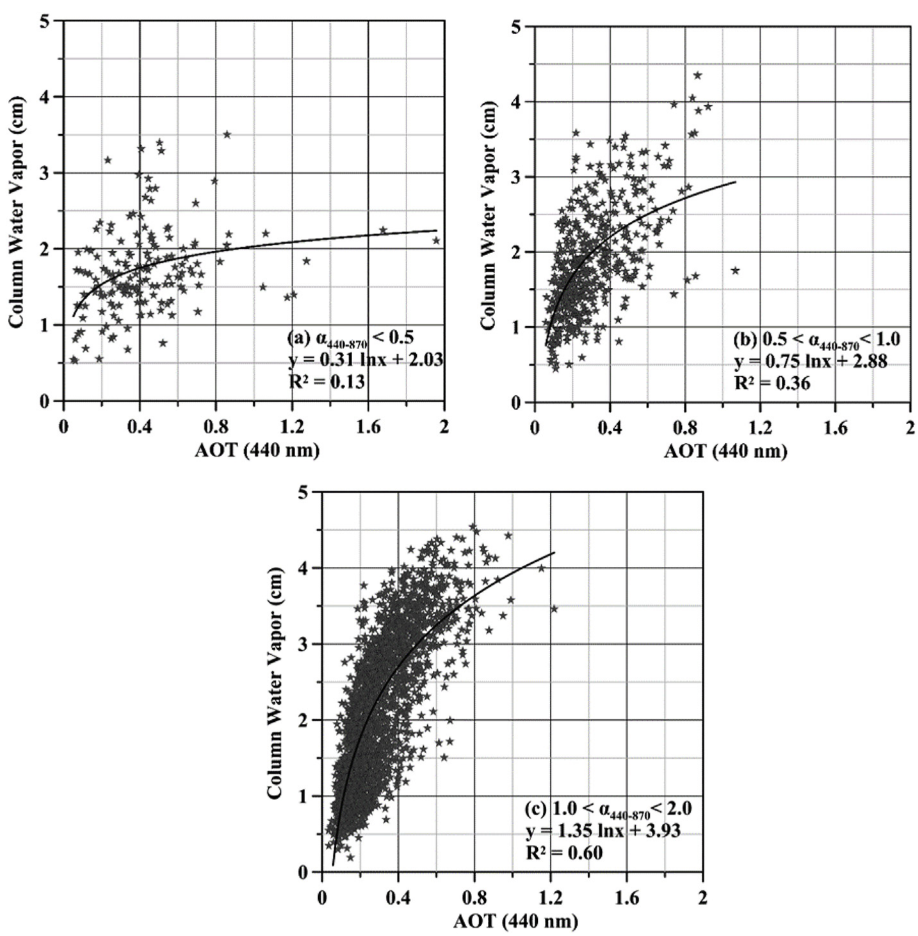

Fig. 9. Aerosol optical thickness versus water vapor with regression analysis for the values of $\alpha_{440\text{-}870} < 0.5$ **(a)**, $0.5 < \alpha_{440\text{-}870} < 1.0$ **(b)**, and $1.0 < \alpha_{440\text{-}870} < 2.0$ **(c)**.

suggested for non-enriched cases, in other words, gypsum mainly arising from dust (Putaud et al., 2004). Regarding, the $nssSO_4^{2-}/nssCa^{2+}$ ratio presented by Koçak et al. (2012) for Erdemli in October 2007 and April 2008, the two individual cases may at least provide further information about the chief aerosol populations of the first and second groups. On 14 April 2008, AOT_{440} and $\alpha_{440\text{-}870}$ were respectively 0.68 and 0.14 whereas AOT_{440} and $\alpha_{440\text{-}870}$ were 0.58 and 0.96 on 11 October 2007, respectively. Correspondingly $nssSO_4^{2-}/nssCa^{2+}$ ratios (Al concentrations) for 14 April 2008 and 11 October 2007 were reported around 0.5 (5.3 $\mu g\, m^{-3}$) and 1.5 (2.6 $\mu g\, m^{-3}$) during these dust events (Koçak et al., 2012), implying that the former event was less interacted with man-made particles than that of observed for later. Consequently, it might be argued that the hygroscopic capacity of the first group was not remarkably modified during long range transport of dust particles into the region.

The coefficient of determination ($R^2 = 0.60$, $p < 10^{-5}$, Fig. 9c) for the last group was strong with a value of 0.60, stating that aerosols associated with this class exhibit a large hydroscopic growth. As stated above, the third category was chiefly associated with hygroscopic fine particles, which may include ammonium sulfate and ammonium nitrate (Tang and Munkelwitz, 1994). Smirnov et al. (2002) have shown similar relationship between AOT_{500} and water vapor for coarse ($R^2 = 0.2$, $\alpha_{440\text{-}870} < 0.7$) and fine ($R^2 = 0.67$, $\alpha_{440\text{-}870} > 0.7$) mode at Bahrain/Arabian Gulf. The increasing trend of AOT_{500} as augmenting water vapor has been reported for a low humid site in Hamim/Arabian Gulf, nonetheless, the relationship between these two variables was found to be independent of aerosol type ($R^2 \sim 0.30$ for both coarse and fine mode, Eck et al., 2008).

In addition to $\alpha_{440\text{-}870}$, OMI-AI was also distinctly different for the three groups (Man-Whitney *U* test $p < 0.002$ for 1st and 2nd groups, $p < 10^{-5}$ for 1st and 3rd as well as 2nd and 3rd groups, see Fig. S12). Correspondingly, arithmetic mean values of OMI-AI were 1.4, 1.1 and 0.8 for the first, second and third groups ($AOT_{440} > 0.4$). Therefore, regarding the difference in the aerosol types, the first, second and third classes were grouped into three categories namely: (a) Non-hygroscopic dominated, (b) moderately hygroscopic and (c) hygroscopic dominated.

Results of PSCF analysis for non-hygroscopic, moderately hygroscopic and hygroscopic aerosols are presented in the maps with a color scale (Fig. 10). Regarding PSCF maps for each group the following observations may be made:

(a) Non-hygroscopic dominated ($\alpha_{440\text{-}870} < 0.5$, Fig. 10a and b; n = 80) Aerosols: As expected, the 80% of such particles were characterized in spring due to the frequent dust intrusions in to the region. The PSCF map for 1 km level indicates the presence of intermediate and strong PSCF valued grid cells in North Africa and the Middle East between coordinates 22°N – 34°N and 8°E – 48°E (Fig. 10a). Particularly, the strong potential probabilities were located at regions covering patches of Southern Tunisia, Western Libya, Libya/Chad border, southern Egypt in North Africa and areas extending from Iraq to eastern Saudi Arabia in the Middle East. On the other hand, the map for 4 km level only shows the major source regions located on North Africa (Fig. 10b). It could be interpreted that mineral dust transported to the region at high altitudes, which was characterized by low angstrom exponent, originated mainly from North Africa. The intermediate and strong PSCF valued cells for 4 km level took place between 16°N-30°N and 10°W-30°E. The map identifies northeastern Mauritania and part of north Mali, southern Algerian Northwestern Niger as strong potential source locations (Fig. 10b). Identified source regions in North African and Middle East are in correspondence with previous studies (Washington et al., 2003; Ginoux et al., 2012, Gherboudj et al., 2017). For instance, Gherboudj et al. (2017) highlighted Chott el-Jerid (Southern Tunisia), Aljafra plain/Nafusa mountains slopes (Tunisia/Libya), Tibesti mountains slopes (Libya-Chad border), river drainage basin of the Aiir (southern Algerian), Erg of Bilma (Northwestern Niger) and Nubian desert (Sudan/Egypt) as important dust emission source areas, which was related to the source regions identified in this study.

(b) Moderately hygroscopic ($0.5 < \alpha_{440\text{-}870} < 1.0$, Fig. 10c and d; n = 110) Aerosols: These particles were almost equally identified in spring (31%), summer (32%) and fall (28%). The PSCF map for 1 km level identifies similar region as the map of 1 km level for $\alpha_{440\text{-}870} < 0.5$. However, a wide area of Western Europe from Spain to Italy and other small areas in France and Germany appeared to be potential source locations (Fig. 10c). These results show that air masses belonging to this group was influenced by both anthropogenic and natural aerosols before reaching to Erdemli (Koçak et al., 2007). As for the PSCF map for 4 km level, region stretching from Northeastern Sudan to Syria were also identified as possible source locations compared to first group's 4 km level PSCF map (Fig. 10d).

(c) Hygroscopic dominated ($1.0 < \alpha_{440\text{-}870}$, Fig. 10 e-f; n = 484) Aerosols: About 80% of the hygroscopic aerosols were observed in summer. The PSCF map for $1.0 < \alpha_{440\text{-}870}$ doesn't clearly show any significant source regions. This may mainly point to the local sources formed under summer conditions. Similar PSCF patterns have been demonstrated for secondary aerosols measured in Erdemli (Koçak et al., 2009).

4. Summary and conclusion

The present study has produced a unique and extensive dataset of temporal aerosol optical and physical properties in the atmosphere over the rural site located at the coast of the Eastern Mediterranean. From these findings the following summary may be made:

Aerosol Optical Thickness (AOT) exhibited log-normal distribution, therefore; AOT is best characterized by it geometric mean concentration, being 15% less than that of arithmetic mean at 440 nm. The arithmetic mean AOT decreased 2.5 times between 440 nm (0.30) and 1020 nm (0.12), demonstrating the dominance of fine particles. Angstrom Exponent ($\alpha = 1.22$), particle size distribution (bi-modal distribution, majority being between 0.1 μm and 0.3 μm) and fine mode fraction (68%) contribution also showed that the aerosol burden was chiefly associated with fine particles.

The lowest AOT values was mainly found in winter during rain or just the day after rain since wet deposition removes aerosol particles from the atmospheric compartment efficiently. Enhanced AOT values at 440 nm was observed in spring with low $\alpha_{440\text{-}870}$ owing primarily to sporadic mineral dust intrusions originated from North Africa and the Middle East. High AOT at 440 nm and $\alpha_{440\text{-}870}$ were principally characterized in summer because of high gas-to particle conversion, sluggish air masses and absence of rain.

Seasonal frequency distribution for AOT at 440 nm exhibited that summer (25% being between 0.3 and 0.4) was more turbid than those of the remaining seasons. 50% of the $\alpha_{440\text{-}870} < 0.5$ in spring was found to be associated with AOT values higher than 0.4, indicating impact of dust transported from deserts located at North Africa and the Middle East. The seasonality of the aerosol optical and physical properties was remarkably modified by water vapor, temperature and rain events. AOT_{440} and AOT_{fine} showed statistically significant negative and positive correlation with rain and temperature, respectively.

Results of air flow categorization for 1 km altitude exhibited that elevated AOT with relatively lower α (0.7) and fine mode fraction (47%) were observed when the air masses originated from North Africa (SAH) and the Middle East (MID). Mean AOT also showed slight decrease between 440 nm and 1020 nm for SAH and MID air flows, denoting importance of coarse mode particles, whereas, this decrease was 65% for air flow from Mediterranean Sea, Eastern Europe, Western Europe and Turkey with comparatively higher α (> 1.1) and fine mode fraction (> 62%).

Regarding the relationship between AOT and Water Vapor (WV) as

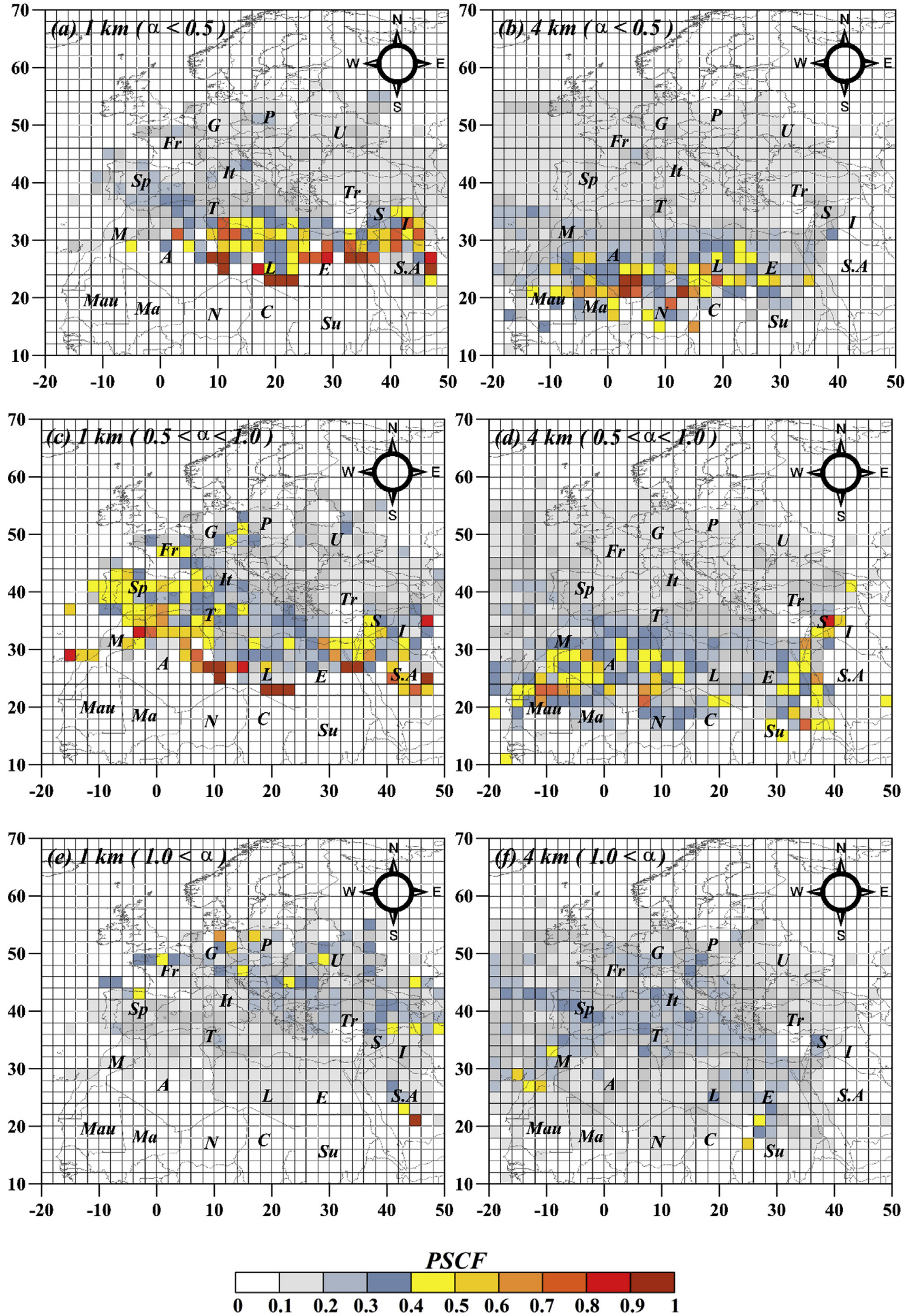

Fig. 10. Distribution of PSCF values at 1 km and 4 km for the values of $\alpha_{440\text{-}870} < 0.5$ **(a–b)**, $0.5 < \alpha_{440\text{-}870} < 1.0$ **(c–d)**, $1.0 < \alpha_{440\text{-}870}$ **(e-f)**. Explanation of abbreviation: Spain (Sp), France (Fr), Germany (G), Poland (P), Ukraine (U), Turkey (Tr), Syria (S), Iraq (I), Saudi Arabia (S.A), Egypt (E), Libya (L),Tunisia (T), Algeria (A), Morocco (M), Mauritania (Mau), Mali (Ma), Niger (N), Chad (C) and Sudan (Su).

a function of α, three classes of aerosol were identified: (a) non-hygroscopic dominated, (b) moderately hygroscopic and (c) hygroscopic dominated. Potential source contribution function (PSCF) maps exhibited that non-hygroscopic particles were associated with mineral dust dominated aerosol population, originating from North Africa (Southern Tunisia, Western Libya, Libya/Chad border, southern Egypt northeastern Mauritania, north Mali, southern Algeria, Northwestern Niger) and the Middle East (extending from Iraq to eastern Saudi

Arabia). Moderately hygroscopic particles, on the other hand, were a mixture of mineral dust and anthropic aerosols due mainly to arrival of the dust after passing through industrialized and populated sites (such as Spain, France and Italy). PSCF maps did not show any particular potential source area for hygroscopic particles, exhibiting nearly mesoscale formation of secondary aerosols under the prevailing summer conditions.

Aerosols play an essential role in precipitation acting as ice and/or cloud condensation nuclei. Most of the non-hygroscopic cases were observed in spring while majority of the hygroscopic cases were characterized in summer. On the other hand, moderately hygroscopic events were almost exclusively uniformly found in spring, summer and fall. Taking into account the origin, composition, air masses history and aging processes, there is a clear need to explore the influence of such particles on the hydrological cycle in the Eastern Mediterranean.

Acknowledge

This study was supported by Middle East Technical University, Project Number: BAP-08-11-2014-021. We acknowledge the GSFC/NASA AERONET group for production of sun photometer data sets used in this research effort. Satellite aerosol optical thickness and aerosol index values from satellite instruments used in this study were produced with the Giovanni online data system, developed and maintained by the NASA GES DISC. We also acknowledge the MODIS and OMI mission scientists and associated NASA personnel for the production of the data used in this research effort.

Appendix A. Supplementary data

Supplementary data to this article can be found online at https://doi.org/10.1016/j.atmosenv.2019.03.007.

References

Barnaba, F., Gobbi, G.P., 2004. Aerosol seasonal variability over the Mediterranean region and relative impact of maritime, continental and Saharan dust particles over the basin from MODIS data in the year 2001. Atmos. Chem. Phys. 4, 2367–2391.
Cadle, S.H., Dasch, J.M., 1988. Wintertime concentrations and sinks of atmospheric particulate carbon at a rural location in northern Michigan. Atmos. Environ. 22, 1373–1381.
Charlson, R.J., Schwartz, S.E., Hales, J.M., Cess, R.D., Coakley, J.A., Hansen, J.E., Hofmann, D.J., 1992. Climate forcing by anthropogenic aerosols. Science 255, 423–430.
Chen, Y., Mills, S., Street, J., Golan, D., Post, A., Jacobson, M., Paytan, A., 2007. Estimates of atmospheric dry deposition and associated input of nutrients to Gulf of Aqaba seawater. J. Geophys. Res. 112, D04309.
Dayan, U., Ricaud, P., Zbinden, R., Dulac, F., 2017. Atmospheric pollution concentrations over the Eastern Mediterranean during summer – a review. Atmos. Chem. Phys. Discuss. 17, 13233–13263. https://doi.org/10.5194/acp-17-13233-2017.
Draxler, R.R., 1999. HYSPLIT4 User's Guide. NOAA Tech. Memo. ERL ARL-230. NOAA Air Resources Laboratory, Silver Spring, MD.
Dubovik, O., King, M.D., 2000. A flexible inversion algorithm for retrieval of aerosol optical properties from Sun and sky radiance measurements. J. Geophys. Res. 105, 20673–20696.
Dubovik, O., Holben, B., Eck, T.F., Smirnov, A., Kaufman, Y.J., King, M.D., Tanre, D., Slutsker, I., 2002. Variability of absorption and optical properties of key aerosol types observed in worldwide locations. J. Atmos. Sci. 59, 590–608.
Dubovik, O., Sinyuk, A., Lapyonok, T., Holben, B.N., Mishchenko, M., Yang, P., Eck, T.F., Volten, H., Muñoz, O., Veihelmann, B., van der Zande, W.J., Leon, J.F., Sorokin, M., Slutsker, I., 2006. Application of spheroid models to account for aerosol particle nonsphericity in remote sensing of desert dust. J. Geophys. Res. 111, D11208.
Eck, T.F., Holben, B.N., Reid, J.S., Dubovik, O., Smirnov, A., O'Neill, N.T., Slutsker, I., Kinne, S., 1999. Wavelength dependence of the optical depth of biomass burning, urban and desert dust aerosols. J. Geophys. Res. 104, 31333–31350.
Eck, T.F., Holben, B.N., Ward, D.E., Dubovik, O., Reid, J.S., Smirnov, A., Mukelabai, M.M., Hsu, N.C., O'Neill, N.T., Slutsker, I., 2001. Characterization of the optical properties of biomass burning aerosols in Zambia during the 1997 ZIBBEE Field Campaign. J. Geophys. Res. 106, 3425–3448.
Eck, T.F., Holben, B.N., Dubovik, O., Smirnov, A., Goloub, P., Chen, H.B., Chatenet, B., Gomes, L., Zhang, X.Y., Tsay, S.C., Ji, Q., Giles, D., Slutsker, I., 2005. Columnar aerosol optical properties at AERONET sites in central eastern Asia and aerosol transport to the tropical mid-Pacific. J. Geophys. Res. 110, D06202.
Eck, T.F., Holben, B.N., Reid, J.S., Sinyuk, A., Dubovik, O., Smirnov, A., Giles, D., O'Neill, N.T., Tsay, S.C., Ji, Q., Al Mandoos, A., Ramzan Khan, M., Reid, E.A., Schafer, J.S., Sorokine, M., Newcomb, W., Slutsker, I., 2008. Spatial and temporal variability of column integrated aerosol optical properties in the southern Arabian Gulf and United Arab Emirates in summer. J. Geophys. Res. 113, D01204.
Eck, T.F., Holben, B.N., Sinyuk, A., Pinker, R.T., Goloub, P., Chen, H., Chatenet, B., Li, Z., Singh, R.P., Tripathi, S.N., Reid, J.S., Giles, D.M., Dubovik, O., O'Neill, N.T., Smirnov, A., Wang, P., Xia, X., 2010. Climatological aspects of the optical properties of fine/coarse mode aerosol mixtures. J. Geophys. Res. 115, D19205.
Fotiadi, A., Hatzianastassiou, N., Drakakis, E., Matsoukas, C., Pavlakis, K.G., Hatzidimitriou, D., Gerasopoulos, E., Mihalopoulos, N., Vardavas, I., 2006. Aerosol physical and optical properties in the eastern Mediterranean Basin, crete, from aerosol robotic network data. Atmos. Chem. Phys. 6, 5399–5413. https://doi.org/10.5194/acp-6-5399-2006.
Gama, C., Tchepel, O., Baldasano, J.M., Basart, S., Ferreira, J., Pio, C., Cardoso, J., Borrego, C., 2015. Seasonal patterns of Saharan dust over Cape Verde – a combined approach using observations and modelling. Tellus B: Chem. Phys. Meteorol. 67 (1), 24410. https://doi.org/10.3402/tellusb.v67.24410.
Gerasopoulos, E., Koulouri, E., Kalivitis, N., Kouvarakis, G., Saarikoski, S., Mäkelä, T., Hillamo, R., Mihalopoulos, N., 2007. Size-segregated mass distributions of aerosols over Eastern Mediterranean: seasonal variability and comparison with AERONET columnar size distributions. Atmos. Chem. Phys. 7, 2551–2561.
Gherboudj, I., Beegum, N., Ghedira, H., 2017. Identifying natural dust source regions over the Middle-East and North-Africa: estimation of dust emission potential. Earth Sci. Rev. 165, 342–355.
Giles, D.M., Holben, B.N., Tripathi, S.N., Eck, T.F., Newcomb, W.W., Slutsker, I., Russell, R., Dickerson, R.R., Thompson, A.M., Mattoo, S., Wang, S.H., Singh, R.P., Sinyuk, A., Schafer, J.S., 2011. Aerosol properties over the Indo-Gangetic Plain: a mesoscale perspective from the TIGERZ experiment. J. Geophys. Res. 116, D18203. https://doi.org/10.1029/2011JD015809.
Ginoux, P., Prospero, J.M., Gill, T.E., Hsu, N.C., Zhao, M., 2012. Global scale attribution of anthropogenic and natural dust sources and their emission rates based on MODIS deep blue aerosol products. Rev. Geophys. 50, 3005.
Haywood, J.M., Shine, K.P., 1995. The effect of anthropogenic sulfate and soot aerosol on the clear sky planetary radiation budget. Geophys. Res. Lett. 22, 603–606.
Haywood, J.M., Shine, K.P., 1997. Multi-spectral calculations of the radiative forcing of tropospheric sulphate and soot aerosols using a column model. Quart. J. Roy. Meteor. Soc. 123 (543), 1907–1930.
Haywood, J.M., Osborne, S.R., Francis, P.N., Keil, A., Formenti, P., Andrea, M.O., Kaye, P.H., 2003. The mean physical and optical properties of regional haze dominated by biomass burning aerosol measured from the C-130 aircraft during SAFARI 2000. J. Geophys. Res. 108 (D13), 8473. https://doi.org/10.1029/2002JD002226.
Holben, B.N., Eck, T.F., Fraser, R.S., 1991. Temporal and spatial variability of aerosol optical depth in the Sahel region in relation to vegetation remote sensing. Int. J. Remote Sens. 12, 1147–1164.
Holben, B.N., Eck, T.F., Slutsker, I., Tanre, D., Buis, J.P., Setzer, A., Vermote, E., Reagan, J.A., Kaufman, Y., Nakajima, T., Lavenue, F., Jankowiak, I., Smirnov, A., 1998. AERONET - a federated instrument network and data archive for aerosol characterization. Rem. Sens. Environ. 66, 1–16.
Holben, B.N., Tanre, D., Smirnov, A., Eck, T.F., Slutsker, I., Abuhassan, N., Newcomb, W.W., Schafer, J., Chatenet, B., Lavenue, F., Kaufman, Y., Vande Castle, J., Setzer, A., Markham, B., Clark, D., Frouin, R., Halthore, R., Karnieli, A., O'Neill, N.T., Pietras, C., Pinker, R.T., Voss, K., Zibordi, G., 2001. An emerging ground-based aerosol climatology: aerosol Optical Depth from AERONET. J. Geophys. Res. 106, 12 067–12 097.
Huang, J., Lin, B., Minnis, P., Wang, T., Wang, X., Hu, Y., Yi, Y., Ayers, J.K., 2006. Satellite-based assessment of possible dust aerosols semidirect effect on cloud water path over East Asia. Geophys. Res. Lett. 33, L19802. https://doi.org/10.1029/2006GL026561.
Husar, R., Prospero, J., Stowe, L.L., 1997. Characterization of tropospheric aerosols over the oceans with the NOAA AVHRR optical thickness operational product. J. Geophys. Res. 102, 16889–16909. https://doi.org/10.1029/96JD04009.
IPCC (Intergovernmental Panel on Climate Change), 2013. The Physical Science Basis, Working Group I Contribution to the IPCC 5th Assessment Report – Changes to the Underlying Scientific/Technical Assessment. Cambridge Univ. Press, New York.
Kaufman, Y., Gitelson, A., Karnieli, A., Ganor, E., Fraser, R., Nakajima, T., Mattoo, S., Holben, B.N., 1994. Size distribution and scattering phase function of aerosol particles retrieved from sky brightness measurements. J. Geophys. Res. 99 (D5), 10341–10356.
Kaufman, Y.J., Tanre, D., Boucher, O., 2002. A satellite view of aerosols in the climate system. Nature 419 (6903), 215–223.
Koçak, M., Kubilay, N., Mihalopoulos, N., 2004. Ionic composition of lower tropospheric aerosols at a Northeastern Mediterranean site: implications regarding sources and long-range transport. Atmos. Environ. 38, 2067–2077.
Koçak, M., Kubilay, N., Herut, B., Nimmo, M., 2005. Dry atmospheric fluxes of trace metals (Al, Fe, Mn, Pb, Cd, Zn, Cu) over the Levantine Basin: a refined assessment. Atmos. Environ. 39, 7330–7341.
Koçak, M., Mihalopoulos, N., Kubilay, N., 2007. Chemical composition of the fine and coarse fraction of aerosols in the Northeastern Mediterranean. Atmos. Environ. 41, 7351–7368.
Koçak, M., Mihalopoulos, N., Kubilay, N., 2009. Origin and source regions of PM10 in the eastern Mediterranean atmosphere. Atmos. Res. 92, 464–474.
Koçak, M., Theodosi, C., Zarmpas, P., Séguret, M.J.M., Herut, B., Kallos, G., Mihalopoulos, N., Kubilay, N., Nimmo, M., 2012. Influence of mineral dust transport on the chemical composition and physical properties of the Eastern Mediterranean aerosol. Atmos. Environ. 57, 266–277.
Koehler, K.A., Kreidenweis, S.M., DeMott, P.J., Petters, M.D., Prenni, A.J., Carrico, C.M., 2009. Hygroscopicity and cloud droplet activation of mineral dust aerosol. Geophys. Res. Lett. 36, L08805.

Kubilay, N., Saydam, C., 1995. Trace elements in atmospheric particulates over the Eastern Mediterranean: concentration, sources and temporal variability. Atmos. Environ. 29, 2289–2300.
Kubilay, N., Nickovic, S., Moulin, C., Dulac, F., 2000. An illustration of the transport and deposition of mineral dust onto the eastern Mediterranean. Atmos. Environ. 34, 1293–1303.
Kubilay, N., Çokacar, T., Oğuz, T., 2003. Optical properties of mineral dust outbreaks over the northeastern Mediterranean. J. Geophys. Res. 108 (D21), 4666. https://doi.org/10.1029/2003JD003798.
Levin, Z., Teller, A., Ganor, E., Yin, Y., 2005. On the interactions of mineral dust, sea salt particles and clouds – measurements and modeling study from the MEIDEX campaign. J. Geophys. Res. 110, D20202.
Lionello, P., Malanotte-Rizzoli, P., Boscolo, R., Alpert, P., Artale, V., Li, L., Luterbacher, J., May, W., Trigo, R.M., Tsimplis, M., Ulbrich, U., Xoplaki, E., 2006. The Mediterranean Climate: an overview of the main characteristics and issues. In: Lionello, P., Malanotte-Rizzoli, P., Boscolo, R. (Eds.), Mediterranean Climate Variability. Elsevier Amsterdam, pp. 1–26.
Mallet, M., Dubovik, O., Nabat, P., Dulac, F., Kahn, R., Sciare, J., Paronis, D., Léon, J.F., 2013. Absorption properties of Mediterranean aerosols obtained from multi-year ground-based remote sensing observations. Atmos. Chem. Phys. 13, 9195–9210 2013.
Marks, R., 1990. Preliminary investigations on the influence of rain on the production, concentration, and vertical distribution of sea salt aerosol. J. Geophys. Res. 95, 22299–22304.
Meloni, D., di Sarra, A., Pace, G., Monteleone, F., 2006. Aerosol optical properties at Lampedusa (Central Mediterranean). 2. Determination of single scattering albedo at two wavelengths for different aerosol types. Atmos. Chem. Phys. 6, 715–727. https://doi.org/10.5194/acp-6-715-2006.
Mihalopoulos, N., Stephanou, E., Kanakidou, M., Pilitsidis, S., Bousquet, P., 1997. Tropospheric aerosol ionic composition in the E. Mediterranean region. Tellus 49B, 1–13.
Moulin, C., Lambert, E., Dayan, U., Masson, V., Ramonet, M., Bousquet, P., Legrand, M., Balkanski, Y.J., Guelle, W., Marticorena, B., Bergametti, G., Dulac, F., 1998. Satellite climatology of African dust transport in the Mediterranean atmosphere. J. Geophys. Res. 103, 13137–13144.
O'Dowd, C.D., Smith, M.H., 1993. Physicochemical properties of aerosol over the northeast Atlantic: evidence for wind-speed related submicron sea-salt aerosol production. Geophys. Res. 98, 1137–1149.
O'Dowd, C.D., Smith, M.H., Consterdine, I.E., Lowe, J.A., 1997. Marine aerosol, sea salt, and the marine sulfur cycle: a short review. Atmos. Environ. 31, 73–80.
O'Neill, N.T., Ignatov, A., Holben, B.N., Eck, T.F., 2000. The lognormal distribution as a reference for reporting aerosol optical depth statistics: empirical tests using multi-year, multi-site AERONET sunphotometer data. Geophys. Res. Lett. 27, 3333–3336.
O'Neill, N.T., Eck, T.F., Holben, B.N., Smirnov, A., Dubovik, O., Royer, A., 2001. Bimodal size distribution influences on the variation of Angstrom derivatives in spectral and optical depth space. J. Geophys. Res. 106, 9787–9806.
O'Neill, N.T., Eck, T.F., Smirnov, A., Holben, B.N., Thulasiraman, S., 2003. Spectral discrimination of coarse and fine mode optical depth. J. Geophys. Res. 108 (D17), 4559–4573. https://doi.org/10.1029/2002JD002975.
Pace, G., di Sarra, A., Meloni, D., Piacentino, S., Chamard, P., 2006. Aerosol optical properties at Lampedusa (Central Mediterranean). 1. Influence of transport and identification of different aerosol types. Atmos. Chem. Phys. 6, 697–713. https://doi.org/10.5194/acp-6-697-2006.
Patterson, E.M., Gillete, D.A., Stockton, B.H., 1977. Complex index of refraction between 300 and 700 nm for Saharan aerosol. J. Geophys. Res. 82, 3153–3160.
Petters, M.D., Kreidenweis, S.M., 2007. A single parameter representation of hygroscopic growth and cloud condensation nucleus activity. Atmos. Chem. Phys. 7, 1961–1971.
Polissar, A.V., Hopke, P.K., Harris, J.M., 2001. Source regions for atmospheric aerosol measured at Barrow, Alaska. Environ. Sci. Technol. 35, 4214–4226.
Prospero, J.M., Ginoux, P., Torres, O., Nicholson, S.E., Gill, T.E., 2002. Environmental characterization of global sources of atmospheric soil dust identified with the nimbus 7 total ozone mapping spectrometer (TOMS) absorbing aerosol product. Rev. Geophys. 40, 1002. https://doi.org/10.1029/2000RG000095.
Putaud, J.P., Van Dingenen, R., Dell'acqua, A., Raes, F., Matta, E., Decesari, S., Facchini, M.C., Fuzzi, S., 2004. Size segregated aerosol mass closure and chemical composition in Monte Cimone (I) during MINATROC. Atmos. Chem. Phys. 4, 889–902. https://doi.org/10.1016/j.rse.2016.04.004.
Rosenfeld, D., Lohmann, U., Raga, G.B., O'Dowd, C.D., Kulmala, M., Fuzzi, S., Reissell, A., Andreae, M.O., 2008. Flood or drought: how do aerosols affect precipitation? Science 321, 1309–1313. https://doi.org/10.1126/science.1160606.
Santese, M., De Tomasi, F., Perrone, M.R., 2008. Advection patterns and aerosol optical and microphysical properties by AERONET over south-east Italy in the central Mediterranean. Atmos. Chem. Phys. 8, 1881–1896. https://doi.org/10.5194/acp-8-1881-2008.
Sciare, J., Oikonomou, K., Favez, O., Liakakou, E., Markaki, Z., Cachier, H., Mihalopoulos, N., 2008. Long-term measurements of carbonaceous aerosols in the Eastern Mediterranean: evidence of long-range transport of biomass burning. Atmos. Chem. Phys. 8, 5551–5563. https://doi.org/10.5194/acp-8-5551-2008.
Smirnov, A., Villevalde, Y., O'Neill, N.T., Royer, A., Tarussov, A., 1995. Aerosol optical depth over the oceans: analysis in terms of synoptic air mass types. J. Geophys. Res. 100, 16639–16650.
Smirnov, A.V., O'Neill, N.T., Royer, A., Tarussov, A., McArthur, B., 1996. Aerosol optical depth over Canada and the link with synoptic air masstypes. J. Geophys. Res. 101, 19299–19318.
Smirnov, A., Holben, B.N., Dubovik, O., O'Neill, N.T., Eck, T.F., Westphal, D.L., Goroch, A.K., Pietras, C., Slutsker, I., 2002. Atmospheric aerosol optical properties in the Persian Gulf. J. Atmos. Sci. 59, 620–634.
Stein, A.F., Draxler, R.R., Rolph, G.D., Stunder, B.J.B., Cohen, M.D., Ngan, F., 2015. NOAA's HYSPLIT atmospheric transport and dispersion modeling system. Bull. Am. Meteorol. Soc. 96, 2059–2077.
Tang, I.N., Munkelwitz, H.R., 1994. Water activities, densities, and refractive indices of aqueous sulfates and sodium nitrate droplets of atmospheric importance. J. Geophys. Res. 99, 18801–18808.
Toledano, C., Cachorro, V.E., de Frutos, A.M., Torres, B., Berjon, A., Sorribas, M., Stone, R.S., 2009. Airmass classification and analysis of aerosol types at el arenosillo (Spain). J. Appl. Meteorol. Clim. 48 (5), 962–981.
Vasconcelos, L., Kahl, J., Liu, D., Macias, E., White, W., 1996. A tracer calibration of back trajectory analysis at the Grand Canyon. J. Geophys. Res. 101 (D14), 19329–19335.
Washington, R., Todd, M., Middleton, N.J., Andrew, S., Goudie, A.S., 2003. Dust-storm source areas determined by the Total Ozone Monitoring Spectrometer and surface observations. Ann. Assoc. Am. Geogr. 93 (2), 297–313.
Xia, X.A., Li, Z.Q., Holben, B., Wang, P.C., Eck, T., Chen, H.B., Cribb, M., Zhao, Y.X., 2007. Aerosol optical properties and radiative effects in the Yangtze Delta region of China. J. Geophys. Res. 112, D22S12. https://doi.org/10.1029/2007JD008859.
Xin, J., Wang, Y., Li, Z., Wang, P., Hao, W.M., Nordgren, B.L., Wang, S., Liu, G., Wang, L., Wen, T., Sun, Y., Hu, B., 2007. Aerosol optical depth (AOD) and angstrom exponent of aerosols observed by the Chinese sun hazemeter network from August 2004 to September 2005. J. Geophys. Res. 112, D05203. https://doi.org/10.1029/2006JD007075.
Yoon, J., Hoyningen-Huene, W., Kokhanovsky, A.A., Vountas, M., Burrows, P.J., 2012. Trend analysis of aerosol optical thickness and Angstrom exponent derived from the global AERONET spectral observations. Atmos. Meas. Tech. 5, 1271–1299. https://doi.org/10.5194/amt-5-1271-2012.